Ultrasonic Velocity Measurements in the Thickness Direction of Paper

C. C. HABEGER and W. A. WINK, *The Institute of Paper Chemistry, Appleton, Wisconsin 54912*

Synopsis

Instruments and techniques for measuring the shear and longitudinal ultrasound velocity through paper in the Z-direction (perpendicular to the plane of the sheet) are described. The fundamental problems in determining elastic properties with ultrasound on thin, rough, fibrous samples are analyzed. Limits are set on sample characteristics, which will assure that the Z-direction velocity measurements are reasonable indicators of Z-direction elastic properties. Data taken over a range of frequencies, pressures, and surface characteristics are presented and analyzed in terms of our concepts of Z-direction wave propagation in paper.

INTRODUCTION

Nondestructive testing of the mechanical properties of paper using ultrasonic techniques is becoming a widespread practice in the paper industry. Early investigations were done in the middle 1960s by Craver and Taylor[1,2] and Jackson and Gavelin.[3] They used a commercial instrument called the Morgan Tester to make in-plane longitudinal and shear velocity of sound measurements in paper. They showed that the elastic stiffnesses calculated from the velocity measurements were sensitive to some major paper machine process variables: refining, wet pressing, and drying tension. Longitudinal velocity determinations in the machine direction (MD) and cross machine direction (CD) were shown to give a quick measure of the elastic anisotropy in paper. They also discovered correlations between longitudinal velocities and tensile strength parameters. More recently, this work was extended at The Institute of Paper Chemistry.[4–10] Here, the Morgan Tester technique of looking at the arrival of a fixed amplitude was improved by measuring the arrival time of a common phase point as a function of transducer displacement. Following the lead of Luukkala et al.,[11] the propagation of high frequency, dispersive plate modes in paper was explained. Velocity measurements in the thickness direction (called the Z-direction or ZD) were made. All nine of the independent elastic parameters of a paper sample were determined from ultrasonic velocity measurements. The effects of paper machine process variables were further investigated. New theoretical and empirical relationships between ultrasonic velocities and strength tests were developed. It was found that ZD velocities were useful in predicting some strength properties. For example, compressive strength was shown to be related to a combination of in-plane and ZD velocities.[10]

At this point the measurement of in-plane ultrasonic velocities is established as a rapid, repeatable, and nondestructive test of paper mechanical

Journal of Applied Polymer Science, Vol. 32, 4503–4540 (1986)
 CCC 0021-8995/86/044503-38$04.00

properties. However, the ZD velocities are intrinsically more difficult to determine. This is because (1) it is difficult to couple ultrasound into the *Z*-direction of the sheet without altering paper properties, (2) the samples are often only the order of one wavelength thick at practical ultrasonic frequencies, and (3) the effects due to surface roughness can cloud the meaning of the measurement. Nonetheless, ZD properties influence the behavior of paper in a number of end-use and converting applications, and the development of reliable ZD velocity measurement techniques is important.

This paper describes the work done over the last few years at The Institute of Paper Chemistry to understand the nature of wave propagation through thin, rough, fibrous samples and to improve the techniques for ZD velocity measurement. It begins with a description of what we now consider to be the best procedures for making ZD longitudinal and ZD shear time-of-flight velocity determinations in paper. Next, techniques for making phase velocity measurements are described. Time-of-flight and phase velocity data taken on a variety of samples are reported and discussed. The results are interpreted, and the limitations of the techniques are analyzed. This paper stresses measurement technique and significance; it does not discuss the practical applications of nondestructive *Z*-direction, ultrasonic testing of paper.

LONGITUDINAL TIME-OF-FLIGHT METHODS

For a time-of-flight measurement, the velocity of a pulse is calculated by dividing the specimen thickness by the pulse transit time. Thus, two measurements are made: transit time and thickness. Paper has very rough, ill-defined boundaries whose average separation varies significantly across the surface. Therefore, to avoid confusion, transit time and caliper measurements are made at the same time and at the same location. To do this, the sample is placed between an ultrasonic transmitter and receiver which are mounted between the anvil and pressure foot of a caliper gage built by Hardacker.[12]

Figure 1 is a schematic of the electronics for measuring the transit time of the ultrasonic pulse. A pulse generator is used to begin each measurement sequence. We have chosen the B&K Model 3020 function generator for our pulse generator. The pulse does two things: It triggers an oscilloscope which displays the transmitter and receiver signals, and it fires a signal generator which activates the ultrasonic transmitter. The pulse generator is adjusted so that the time between pulses is less than 15 ms and greater than 300 μ. The repetition time is less than 15 ms to avoid flicker in the oscilloscope display; it is greater than 300 μs to insure that all reverberations from the previous pulse have died out before firing another pulse. The signal generator, Interstate Model F77, is adjusted to produce a single cycle of a sine wave upon the receipt of the trigger pulse. The amplitude and initial phase of the signal generator output are adjustable. The largest possible amplitude is chosen without saturating the preamplifier. Normally there is no saturation when the signal generator runs at its maximum output of 15 V peak to peak. The phase adjustment is discussed later.

The signal generator output excites a piezoelectric transmitter which generates a mechanical longitudinal pulse. The signal generator output is also routed to channel A of the oscilloscope which is operated in the alternate

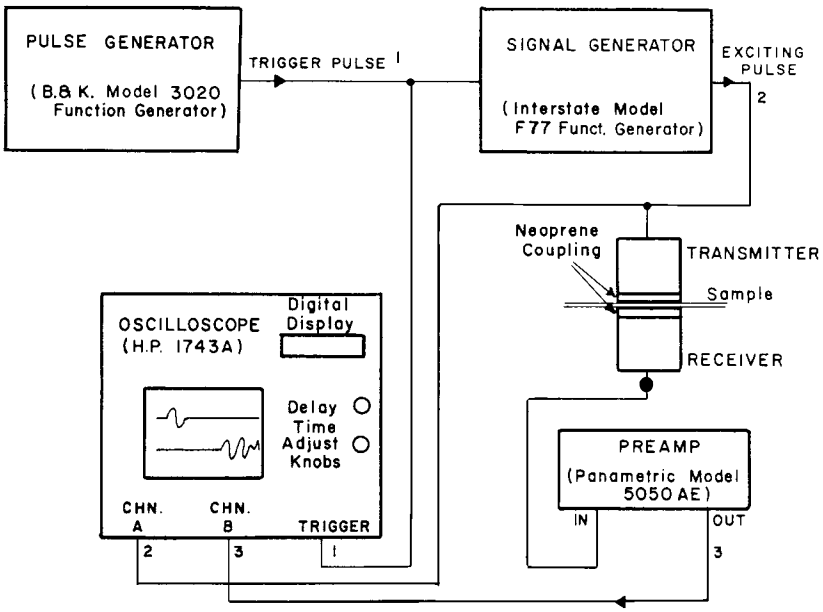

Fig. 1. Schematic for the ZD longitudinal time-of-flight velocity measurements.

mode. The mechanical pulse propagates through the sample to a receiver transducer which produces an electrical output. This output is amplified by a battery-powered preamplifier, Panametrics Model 5050AE, and displayed on channel B of the oscilloscope.

The oscilloscope, a Hewlett-Packard Model 1743A, accurately determines the time between selected features on the A and B traces. When in the main operating mode, a cursor (a section of the trace brighter than the rest) can be displayed on each trace. The positions of the two cursors can be independently aligned by using the delay time adjustment knobs. A digital display on the front panel of the oscilloscope reads out the time difference between the two cursors in nanoseconds. To assign a time of arrival to the pulse on channel B, the cursors are adjusted to cover the firing pulse on channel A and the beginning of the received pulse on channel B. When the oscilloscope is changed from the main mode to the delayed mode, only the cursor regions are displayed. However, the digital display still gives the time difference of the two cursor regions. The display knobs are adjusted so that the first pulse in the received signal aligns with the transmitter pulse on channel A. In actual operation the vertical positions and vertical gains are adjusted until the two traces overlap. With this technique, a sensitive and repeatable time can be associated with the arrival of the received pulse.

The longitudinal transducers were designed and built at The Institute of Paper Chemistry specifically for coupling ultrasound into paper in the *Z*-direction. The active element in each transducer is a piezoelectric ceramic (PZT 5A) disk, 2.54 cm in diameter and about 0.25 cm thick. Its resonant frequency is 2.25 MHz. The backside of the active element is epoxied to a ballast pellet to increase the bandwidth of the transducer. The ballast was made from a mixture of about 95% powdered tungsten and 5% silicone potting compound (General Electric RTV 615). The pellet was formed by

pressing the mixture to 8.6×10^8 N/m^2 and allowing the potting compound to cure. The final diameter of the pellet was 2.54 cm and its thickness was about 1.2 cm. The pellet was a high density (~13 g/cm^3), high loss substance and thereby a good absorber for the high density lead zirconate titanate piezoelectric transducer. The front surface of the active element was epoxied to a fused silica delay line, about 3.5 cm in diameter and 3.8 cm long.

The purposes of the delay line are (1) to separate the shear waves and longitudinal waves in time so that the longitudinal signal has no shear interference and (2) to provide a delay line of sufficient length to contain a pulse of at least 5 cycles for use in the phase velocity measurements to be described later. The ends of the fused silica cylinders were hand polished until they were flat within about 2 μm. The delay line is mounted to a brass housing which encloses the active element. The housing provides electrical shielding and electric connection through a BNC connector mounted on its side. The transducers are broad-banded enough to allow transit time measurements from about 1.0 to 2.0 MHz. However, they still ring, and signals from multiple delay line reflections continue for about 150 μs after the initial pulse.

The hard, flat, fused silica surfaces are not acceptable for measurements on paper surfaces. One reason for this is that an artificially large caliper is obtained when paper is placed between hard surfaces. The hard platens make contact only at the high points of the paper surface, and their separation is greater than the average displacement between the boundaries. A more reasonable measure of caliper is made when soft neoprene platens (~0.08 cm thick "super soft neoprene" of 5–10 durometer from Crane Packing Co.) are used. The neoprene platens conform to the rough paper surfaces and thereby yield a caliper which is closer to the average distance between the paper surfaces. A discussion of this technique and a comparison of its results with those of other caliper measurements are given in an article by Wink and Baum.[13]

Obtaining a sensible caliper is not the only reason for using a neoprene buffer between the delay line and the sample. The delay line does not effectively couple acoustic energy directly into the paper. The fused silica has a high mechanical impedance (~ 1.3×10^7 kg/m^2 s), whereas paper has a very low ZD impedance (~ 3.5×10^5 kg/m^2 s); therefore, almost all of the acoustic energy would be reflected even at a well coupled fused silica-to-paper interface. The problem is compounded, since standard methods of coupling a transducer to a specimen are unacceptable in the case of paper. Generally, a viscous fluid or epoxy bond is used to make the couple. Both of these lead to gross changes in the properties of the paper sample and must be ruled out. The neoprene buffer is a good solution to the coupling problem. It conforms to the rough sample surface and couples effectively without altering the sample. It is of intermediate impedance and reduces the reflection losses. The neoprene is epoxied to the delay lines of the longitudinal transducers.

The first step in measuring the ZD longitudinal velocity of a sample is to place the proper weights on the pressure foot to give the desired pressure at the sample. The most commonly used pressure is 50×10^3 N/m^2, the TAPPI standard (Method T 411) pressure for making caliper measurements.

Other values have been used, and the effects of pressure are described later. Once the weights are in place, a representative specimen is inserted, and the pressure foot is lowered. The phase of the signal generator is adjusted so that a distinct half cycle is visible at the beginning of the received pulse. One such phase adjustment is usually sufficient for testing a series of samples.

Before transit times are recorded, an aluminum foil sample is used to determine the baseline time, T_B. This is the time required for the signal to pass through the electronic circuits and sensors without a sample. The foil is used because the neoprene deforms differently when in contact with a sample than it does when in contact with another piece of neoprene. When under pressure, the edge of the neoprene forms an arc. There is a single arc when the neoprene surfaces are in contact, but two separate arcs appear if a sample is in place. The effective thickness of the two layers of neoprene is less when in direct contact with each other than when a sample is inserted. The solution to this problem was to put a piece of flat aluminum foil (~10 μm thick) between the neoprene surfaces. Now the neoprene is deformed as if a paper sample were in place. The transit time with foil is found by aligning the transmitted and received pulses on the oscilloscope, as described previously. The ZD velocity of sound is higher in aluminum (6420 m/s) than in typical paper (~400 m/s); therefore, the foil transit time is relatively small. To get T_B, a correction is made by subtracting 6420 m/s multiplied by the foil caliper (usually less than 3 ns) from the total transit time with foil. Once T_B is determined, it can be used as long as the phase and frequency settings are unaltered; however, it is periodically checked so that any drift in the electronic circuitry does not result in errors.

Now a specimen is placed between the sensors, and the pressure foot is lowered. It is necessary to wait about 10 s for the caliper and transit times to stabilize. The transit time T_P is taken from the digital display when the first half cycle of the received wave is aligned with the transmitting cycle in exactly the same way T_B was determined. The caliper (D) is recorded, and the velocity is equal to $D/(T_P - T_B)$. Sheet properties can vary considerably over the expanse of the sample; therefore, readings are averaged from a number of sensor locations. Generally about six readings are taken on a 10 × 10 cm sample.

SHEAR TIME-OF-FLIGHT METHODS

Time-of-flight, ZD, shear velocity measurements are similar to the longitudinal tests. Velocity is calculated from caliper divided by transit time while the specimen is held in a caliper gage. The differences are in sensor construction, coupling, and the baseline measurement. At present there are two techniques for determining shear velocity. One is relatively tedious and is used on thin or rough samples. The other is a straightforward procedure similar to the longitudinal test.

The direction of oscillation of a shear transducer is in the plane of the surface. This, of course, is counter to a longitudinal transducer where motion is along the normal. Longitudinal transducers are made by aligning the electric field in the direction of polarization. To produce shear motion on

the transducer surface, the electric field is applied perpendicular to the direction of transducer polarization. The shear motion is in the plane determined by the polarization and field.

The transducers used for shear measurements were custom built by Ultran Laboratories, Inc. The active element in the transducers is a plastic piezoelectric material. There is a ballast on the back side for bandwidth broadening. Provisions are made for attaching delay lines to the front of the transducers. This is accomplished by means of a threaded cap with a center hole so the front of the delay line can protrude. Polystyrene, polypropylene, and polyethylene delay lines have been tried; the polystyrene was selected because it couples more energy into the sheet. Delay lines are essential, since shear transducers also have a significant longitudinal impurity. The delay lines allow the longitudinal signal to die out before arrival of the shear signal. The delay lines are flanged on the back side so they can be clamped between the cap and front wear face of the piezoelectric transducer. The front of the piezoelectric element is 1.27 cm in diameter, and the delay line is 1.43 cm in diameter at the front and 1.27 cm long. The faces of the delay lines have been surface ground and are flat to 1 μm. The perimeters of the delay lines are grooved to reduce the generation of high-order modes upon surface reflection. Each delay line is coupled to its piezoelectric element by applying a thin layer of SWC shear couplant (from Panametrics Inc.) and tightening the knurled, threaded cap by hand. The transducers are mounted in a caliper gage with the shear motion parallel to the front edge of the gage.

The reason that the shear transducers were made with plastic piezoelectric materials and plastic delay lines is that shear waves are difficult to couple into paper. The rubber interface used in the longitudinal gage is not practical here, since the rubber does not effectively transfer shear waves into the sheet. Without epoxy or a viscous coupling fluid, normal high impedance transducers do not introduce sufficient shear energy into paper samples. The solution was to procure transducers and make delay lines with lower mechanical impedances. This reduced reflections at the transducer–specimen interfaces and thereby increased the transfer of signal through the sample. The transducers described above provide sufficient signal without a couplant and can be used for time-of-flight measurements at frequencies of 0.5–1.0 MHz. Unfortunately, this means that caliper is still measured with hard platens and that the ultrasonic signal is transferred through the peaks of the paper surface which are in contact with the delay lines. As will be shown later, this gives an acceptable velocity for smooth paper surfaces but leads to unreasonably high velocities for extremely rough samples (e.g., corrugating medium).

The straightforward shear technique uses the bare delay lines for specimen contact. The procedure for finding caliper and transit time with a specimen is identical to the longitudinal test which has been described. In this case, however, it is not necessary to use the aluminum foil; the baseline time is taken with nothing between the delay lines. After repeated contact with paper, grit and/or paper debris can build up on the polystyrene surfaces. Periodic cleaning is done by inserting aluminum foil between the sensors, lowering the upper probe, and rotating the foil back and forth through about

15°. This is repeated with fresh foil until there is no sign of wear on a spent foil. The foil must be degreased by dipping it in carbon tetrachloride before use.

Machine-made paper has a different ZD shear velocity when the shear polarization is in the MD than when it is in the CD. The velocity in the MD–ZD plane is about 10% to 20% greater than in the CD–ZD plane. This is not as large as the in-plane longitudinal anisotropy, where V_{MD} is about 30–60% greater than V_{CD}. The shear velocity in the MD–ZD plane is determined by aligning the specimen's MD along the front edge of the gage. The CD–ZD shear measurement is realized by rotating the sample 90°.

Although the bare transducers are acceptable when the surface variations are small compared with the caliper, gross errors result on rough samples, and ZD longitudinal to shear velocity comparisons are clouded, since different calipers are used. The ideal solution is to find a shear couplant that will conform to rough surfaces as well as soft neoprene but that will not penetrate the sheet or alter its mechanical properties. Our solution is a viscous fluid couplant encapsulated between thin polymer films. The fluids used are polybutenes. Different viscosities are realized by using different molecular weight distributions. In practice, the viscosity is between 0.2 and 7.4 kP. The effective shear modulus of a viscous fluid is $i\omega\mu$, where $i = (-1)^{1/2}$, $\omega = 2\pi$ times the frequency, and μ = viscosity. At 1 MHz the absolute values of the shear moduli of the fluids range from 1.3×10^8 to 4.7×10^9 N/m^2. Thus, the fluids are quite rigid in shear at ultrasonic frequencies, and the fluid film "pillows" provide conformable, yet stiff, shear coupling. The encapsulating film should be thin and conformable, yet free of pin holes and easily sealed. After many trials, we chose a low density polyethylene film made by Ethyl Corp., VisQueen Division. It is about 14 μm thick and is treated on one side with a corona discharge. The "pillow" method reduces the error that results from poor coupling and should always be used when the surface is rough. In addition, the improved coupling leads to an order of magnitude increase in signal amplitude; therefore, the pillows are also useful for thick samples where sufficient signal cannot be passed with hard contact.

The construction of a film–fluid pillow is described below. A disk of polymer film 3.2 cm in diameter is punched out with the corona-treated side up, and it is placed on top of a cylinder of 2.54-cm diameter. The cylinder has a raised rim about 0.16 cm wide around its perimeter. This forms a small reservoir into which 0.09 cm^3 (approximately 72 mg) of the viscous fluid is deposited. Next a layer of Miller Stephenson 907 epoxy is metered onto a flat glass plate. A film of epoxy is transferred to the rim of another aluminum cylinder identical to the one above. From here, the circle of epoxy is transferred to the corona-treated side of another piece of film about 3.8 cm^2. The machine direction of this film has been marked. It is placed, epoxy side down, over the first piece of film so that the machine directions of the two films are aligned and the epoxy circle coincides with the rim. Another cylinder is now placed on top of the pillow so that the two rims and epoxy circle are aligned. The assembly is weighted with about 1 kg and allowed to sit overnight to cure the epoxy. Pin holes are rarely found in the film, and the resulting epoxy sealed "pillows" are clean and conformable couplants. These

pillows provide an effective acoustic interface between the polystyrene delay lines and the sample.

Although the pillow method greatly reduces the coupling problem, it introduces some new difficulties. When a load is applied to a sample between pillows, the fluid flows to the pillow edge away from the delay line. Initially, an excess of fluid exists in the loaded region. After a time, which depends on fluid viscosity and surface roughness, the fluid in the loaded region is nearly depleted. This leaves the following questions to be answered: At what point in this dynamic process should the transit time be taken? What is the caliper at this point? How is the baseline time measured?

If the received signal is monitored during the outflow of viscous fluid, the signal amplitude increases initially and the transit time decreases. The signal amplitude peaks at a time that varies with sample roughness and fluid viscosity. After this the signal amplitude falls off and the transit time decreases very slowly. In some cases (smooth samples and high viscosity fluids), the signal seems to plateau and does not decrease in reasonable time periods. For all samples tested, it was possible to select a polybutene fluid that resulted in convenient peak times. We presume that below the signal peak there is an overabundance of fluid between the sensors. This causes less than optimum coupling and a less than optimum signal. When the signal peaks, there is a thin layer of fluid between the polymer film boundaries. After the signal peaks, the polymer films begin to come in contact with each other, and the fluid coupling is lost. At the signal peak, the fluid has complete but minimal coverage. This is the point at which to measure transit time for the sample. Pillows are chosen so that 0.5–3-min peak times are achieved for the given sample. Higher viscosity fluids are used on rougher surfaces.

Now, what is the paper caliper at the time the signal peaks? At the peak signal, we assume that there is complete fluid contact with the polymer film and that the film conforms to the paper surface as well as possible at the applied pressure. The way to reproduce this state in the paper and the film is to insert a sample sandwiched between single polymer films into a neoprene platen caliper gage. The neoprene will force the film to comply with the paper surface in essentially the same manner as the fluid. Thus, the caliper is the thickness of the sample and two sheets of polymer film in a neoprene caliper gage minus the thickness of the two films. The caliper so calculated is larger than the neoprene caliper, because the polyethylene film is less conformable than neoprene. However, it is much closer to the soft neoprene caliper than is the caliper obtained between hard platens.

To find the baseline time T_B without a sample present, the transit time must be measured with the same amount of fluid in the pillows as at peak signal, but with no sample. The thickness of the two pillows at peak signal can be calculated by subtracting the caliper of the paper between the films and neoprene from the caliper gage reading at peak signal. The baseline time is measured by putting two pillows between the delay lines and applying a load. The transit time, when the caliper gage reads the same value as the two-pillow thickness at peak signal, is the baseline time. Often, transit time is plotted vs. displacement, and T_B is taken as the time regressed to the two-pillow caliper at the peak signal. There are always points on both

sides of the regressed value. After some use, the baseline may drift, but cleaning the pillows (described later) will restore the baseline to its original value.

To evaluate the dependence of the "pillow method" velocities on fluid viscosity, tests were performed on samples of three different roughnesses over a range of pillow fluids. The samples were a corrugating medium, the same medium with a small amount of surface grinding, and the same medium ground to a smooth surface. The computed velocity was independent of viscosity, and a fluid was available to reach the peak signal in a convenient time, except for the very smooth surface. The data also indicated that velocities can be taken from peak plateaus as well as peaks if necessary.

The polyethylene films are thin and compliable; therefore, they must be handled gently on the outer edges with tweezers. When subjected to a significant tension, stretching and work-hardening can occur. This causes changes in the film caliper and the measured ultrasonic delay time. If any stretching is suspected, the baseline should be redetermined. The films are anisotropic, and the delay time for a shear wave in the ZD–MD plane is less than that in the ZD–CD plane. Therefore, the alignment of the film machine direction with the direction of polarization of the transducers must be the same for all baseline and sample measurements.

The step-by-step procedure for making ZD shear velocity measurements with the viscous fluid pillows is summarized here.

1. Measure the thickness of the sample between polyethylene film and neoprene. One thickness of film is placed on each side of the sample. The MD of the film is aligned in the direction of polarization of the transducers for both ZD–MD and ZD–CD shear measurements. Each test area must be identified so the subsequent ultrasonic measurement can be made in the same test areas. Record the combined thickness of sample and film, D_{NP}, for each area measured.

2. Ultrasonic time-of-flight measurements are made in the identified areas with the sample placed between two pillows. The function generator is set at the chosen frequency (usually 1.0 MHz), and the phase is adjusted to give a prominent first half cycle. Before inserting the sample and pillows into the caliper gage, the fluid is concentrated in the center of the pillows. This is done by centering a pillow over a 1.25-cm hole in a piece of rubber and loading the pillow with a cylinder having a 1.25-cm recess. The load is a few hundred grams applied for about 10 s. Insert the sample with a pillow on each side into the caliper gage. The film MD should be aligned in the transducer polarization direction. The sample is aligned with the sensor polarization in the plane of test. With the pillows and sample in the caliper gage, lower the pressure foot. Wait for the maximum ultrasonic signal (or maximum signal plateau in the case of relatively smooth-surfaced materials). At the maximum signal, observe and record the distance (D_U) from the digital display on the thickness gage and the time interval (T_U) from the digital display on the oscilloscope, in the same manner as in the longitudinal case. The time required to reach the maximum signal depends on the surface roughness of the sample and on the viscosity of the fluid. A fluid that will give rise to a maximum signal in 0.5–3 min should be selected.

3. Calculate the baseline distance (D_B) for the two pillows that were used for the measurement of step 2, using the following equation:

$$D_B = D_U - D_{NP} + 2D_P \tag{1}$$

Here, D_P is the thickness of a single piece of the film, a value derived from the measurement of four thicknesses of film between neoprene.

4. Find the baseline time (T_B). Place the two pillows (film MD aligned with sensor polarization) between the shear sensors. Load until the separation is D_B and record the time T_B. As an alternative, T_B can be determined by plotting T vs. D and extrapolating T_B at D_U. Because of instabilities in the electronics it is wise to check this step after each six to ten measurements of step 2.

5. Compute the shear velocity using the following equation:

$$V = (D_U - D_B)/(T_U - T_B) \tag{2}$$

6. As needed, clean the polystyrene delay lines with degreased aluminum foil as described earlier. Also, a significant amount of drift in the baseline time will occur if the polystyrene and the polyethylene surfaces are not routinely cleaned with a solvent. Our cleaning solution is produced by diluting 1.5 mL of MICRO Laboratory cleaning solution (International Products Corporation) with 100 mL of water. Contaminated surfaces are immersed for 1.0–2.0 min, rinsed in water, and blotted dry with tissue. Care should be taken not to rub the pillows with the tissue.

The pillow method is a very tedious procedure, and (as will be seen later) it is necessary only on very rough samples.

PHASE VELOCITY TECHNIQUES

The delay lines on the shear and longitudinal transducers permit phase velocity measurements as well as the time-of-flight velocity measurements just described. The delay lines are long enough to contain a burst of over 10 cycles at the lowest frequencies used. Thus, if a short burst of sine waves (an rf pulse) excites the transmitter, a discrete pulse of energy is momentarily completely contained in the delay line. When it hits the sample, the rf pulse is decoupled from the active element in the transmitter. The leading edge of the rf pulse is distorted, but after a few cycles its shape is again sinusoidal with constant amplitude. When equilibrium is approached, the relationship between the signal transferred through the sample to the receiver (E_T) and the portion reflected by the delay line–sample interfaces (E_R) can be found by assuming that the delay lines are infinitely long and that the signal is a continuous wave. That is, the phase shift and amplitude ratio of E_T relative to E_R are calculated from standard transmission line equations, using the characteristic impedances of the delay lines and the samples and the sample caliper.

The advantages of phase velocity measurements over time-of-flight measurements are (1) the effects of multiple reflections at the sample-delay line interfaces can be accounted for and (2) distortions in the initial shape of a

wave packet, due to dispersion in the sample, do not cause errors. The time-of-flight technique assumes that the first peak comes straight through the sample with no distortion. The phase velocity method considers the signal to be a continuous wave and mathematically accounts for the interferences from multiple reflections. Distortion problems are avoided by looking far enough into the pulse that the signal can be approximated as a pure sinusoid. In time-of-flight measurements, the effects of multiple reflections do not become significant until the caliper is less than about one-eighth of a wavelength. When the caliper is this small, a component reflected back and forth through the sample one time and then through to the receiver could interfere with the first peak of the straight-through component. Since ZD velocities are generally less than 600 m/s and the lowest frequency used is 0.5 MHz, time-of-flight errors from multiple reflection are of concern only for calipers less than 150 μm. The importance of distortion errors are harder to assess. However, it will be argued later that distortion and multiple reflection problems are small compared with errors coming from surface roughness and poor coupling. These difficulties affect time-of-flight and phase velocity methods equally.

Our first phase velocity technique was taken from work done by McSkimmin[14] over 30 years ago. Here, the real and imaginary parts of the elastic stiffness are found by comparing E_T to E_R in the equilibrium region. From a transmission line calculation, McSkimmin gives the ratio as

$$E_R/E_T = \tfrac{1}{2}(Z_S/Z_T - Z_T/Z_S)\sinh(ik_s l_s) \tag{3}$$

where Z_T is the delay line impedance, Z_S is the complex impedance of the sample, i is $(-1)^{1/2}$, k_s is the complex wave number of the sample, and l_s is the caliper. If the density (ρ_s) is measured, Z_S can be calculated from k_s and the angular frequency (ω):

$$Z_S = \rho_s\omega/k_s \tag{4}$$

Since k_s is complex, there are two unknowns on the right-hand side of eq. (3). If the phase and amplitude of E_p/E_T are measured, eq. (3) becomes two simultaneous, transcendental equations with two unknowns. Therefore, if the phase shift between E_T and E_R is known to within one cycle, k_s can be determined. Once k_s is known, the phase velocity (V_P) and the complex elastic stiffness (C_S) are calculated as in

$$V_P = \omega/\mathrm{REAL}(k_s) \tag{5}$$

$$C_S = \rho_s\omega^2/k_s^2 \tag{6}$$

From eq. (3) it is clear that the phase difference between E_T and E_R is carrier-frequency-dependent. As frequency varies, the phase difference progresses continuously, and the signals alternate from in-phase to out-of-phase. At the discrete frequencies where E_T and E_R are exactly in-phase or out-of-phase, eq. (3) simplifies to eqs. (7) and (8).

$$\frac{E_R}{E_T} = \frac{1}{2Z_T\rho_s\omega}\,[B(|Z_S|^2 - Z_T^2)(\sinh Al_s \cos Bl_s) - A(|Z_S|^2 + Z_T^2)(\cosh Al_s \sin Bl_s)] \quad (7)$$

$$B(|Z_S|^2 - Z_T^2)\cosh Al_s \sin Bl_s = -A(|Z_S|^2 + Z_T^2)(\sinh Al_s \cos Bl_s) \quad (8)$$

The symbols A and B are defined by $ik_s = A + iB$. McSkimmin[14] solved eqs. (7) and (8) graphically. We use a computer program that performs an iterative search for the roots of the equations. Thus, eqs. (7) and (8) can be used to calculate the complex elastic modulus at the special frequencies where E_T and E_R are in-phase or out-of-phase. This phase requirement limits the measurement to samples with calipers greater than about 100 μm.

The actual McSkimmin measurements are made using a pulse generator, a signal generator, an oscilloscope, and a counter. The pulse generator and signal generator are used to apply a pulsed rf signal (1–3 MHz) to the transmitting transducer and to trigger the oscilloscope. One oscilloscope channel is connected to the transmitting transducer and the other to the receiver. The frequency of the pulsed rf is adjusted so that the reflected and transmitted pulses are exactly in- or out-of-phase. These relationships are detected by putting the oscilloscope in the mode that adds the two channels. An out-of-phase condition is found by adjusting the gain of one channel and the rf frequenccy until an oscilloscope null is reached. The in-phase condition uses the same process, but one channel is inverted by the oscilloscope. The frequency at null is read from a counter, and the ratio of the two signal magnitudes is taken from the oscilloscope. This information, along with sample caliper and basis weight, is fed to the computer and it calculates the velocity and loss tangent, using eqs. (7) and (8).

Poor coupling between the hard longitudinal delay lines and the sample leads to problems with the McSkimmin technique. In the derivation of eq. (3), it was assumed that the sample was a homogeneous material, well-bonded to the delay lines. The stresses and velocities at the boundaries were taken to be continuous. McSkimmin used smooth plastic samples which were coupled to the delay lines with a viscous coupling film much thinner than the plastic thickness. A firm contact was thus achieved with a small change in the samples' mechanical properties. We have ruled out the use of coupling fluids because of their large effect on paper properties. For longitudinal measurements coupling errors can be reduced by using the soft neoprene to couple the delay line and the sample. This also gives a more realistic measure of the caliper and density.

The use of rubber platens with the McSkimmin technique, however, requires a refinement of eq.(3). The neoprene platens are treated as uniform transmission lines with a known impedance (Z_R), wave number (k_r), and thickness (l_r). The relationship between E_R/E_T with neoprene coupling can now be derived from acoustic transmission line equations. Specifically, rearranging and simplifying some relations given by Hill and El-Dardiry[15] (see Appendix A) leads to eq. (9) as the replacement for eq. (3):

$$\frac{E_R}{E_T} = \frac{i}{2} S_S C_R^2 \left(\frac{Z_s}{Z_T} - \frac{Z_T}{Z_s}\right) + \frac{i}{2} S_S S_R^2 \left(\frac{Z_S Z_T}{Z_R^2} - \frac{Z_R^2}{Z_S Z_D}\right) + iC_S C_R S_R \left(\frac{Z_R}{Z_T} - \frac{Z_T}{Z_r}\right) \tag{9}$$

Here $C_R = \cos k_r l_r$, $S_R = \sin k_r l_r$, $C_S = \cos k_s l_s$, and $S_S = \sin k_s l_s$. Once the acoustic impedance, the thickness, and density of the neoprene element are measured, the mechanical properties of the sample can be calculated from E_R/E_T, as in the usual McSkimmin method. The neoprene we used had a thickness of 8.74×10^{-4} m and a density of 1108 kg/m^3. From a McSkimmin measurement on a neoprene sample, the impedance was found to be 1.65×10^6 kg/ms^2. The imaginary part of the neoprene impedance was judged to be small (compared to the real part) and was set equal to zero.

Velocities measured with the McSkimmin technique generally agree well with the time-of-flight velocities when the caliper is over 100 μm. As an example, look at the series of variable basis weight, bleached kraft sheets shown in Figure 2. The McSkimmin and time-of-flight values using neoprene are within the experimental error, whereas the hard platen, time-of-flight numbers are significantly lower. This probably means that the effect of multiple reflection is not significant for these time-of-flight measurements. This does not mean that no errors arise from insufficient sample to delay line coupling. It merely means that any coupling complications are affecting both measurements in approximately the same way. Since time-of-flight and McSkimmin velocities are equivalent, the subsequent results

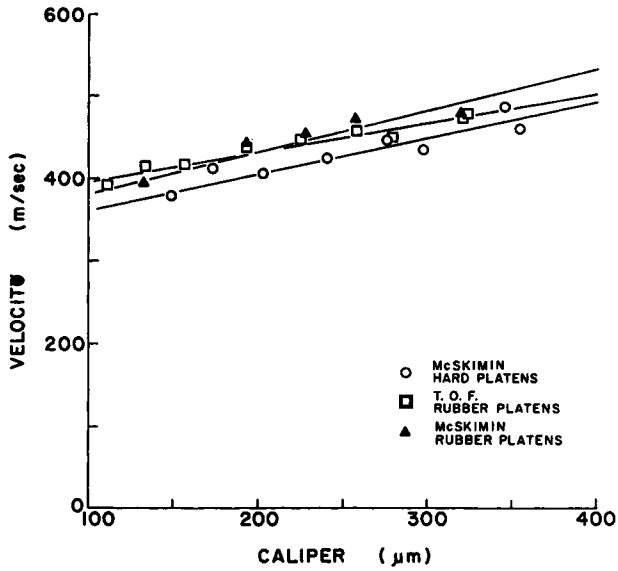

Fig. 2. Longitudinal ZD velocity vs. caliper for a series of variable basis weight, bleached kraft handsheets made to an approximately equal apparent neoprene density (0.771 ± 0.006 g/cm^3): (○) McSkimmin hard platens; (□) TOF rubber platens; (▲) McSkimmin rubber platens.

reported here will generally be the more easily measured time-of-flight values. The question of coupling error in ZD velocity measurements will be discussed later.

Another interesting feature of the McSkimmin technique is that it gives the loss tangent (tan δ) as well as the velocity. The value of the calculated loss tangent is much more sensitive to coupling quality than is the velocity value, making interpretation of the results more difficult. Poor coupling results in an overestimation of the loss tangent. Accurate values of the loss tangent are determined only if the sample is epoxied to the delay line or if a very viscous coupling fluid is used. Such couplings could change the properties of paper, however, and should not be used. We had hoped that the neoprene McSkimmin methods would provide sufficient coupling. The coupling is improved by using neoprene platens as seen in Figure 3, where the loss tangent for the variable basis weight samples is plotted vs. caliper. Three sets of data are given: neoprene platen longitudinal, hard platen longitudinal, and hard platen shear. The hard platen numbers are much greater than those obtained using the neoprene, presumably due to better coupling with the neoprene. The tan δ values are still believed to be too high, however. This is supported by results obtained on thin plastic disks, tested with neoprene platens and with hard platens. The hard platens were coupled to the plastic sample in three different ways: with vacuum grease, with a very viscous couplant, and with epoxy. The epoxy and viscous couplant data for tan δ were near the handbook values for the plastic, whereas the vacuum grease and neoprene results were 2.5 times greater. If the neoprene gives high values when coupled to smooth plastic surfaces, the values found for a rough surface paper sample must be much greater than the real loss tangent. In summary, the McSkimmin method was not very successful in measuring loss tangent for the paper samples.

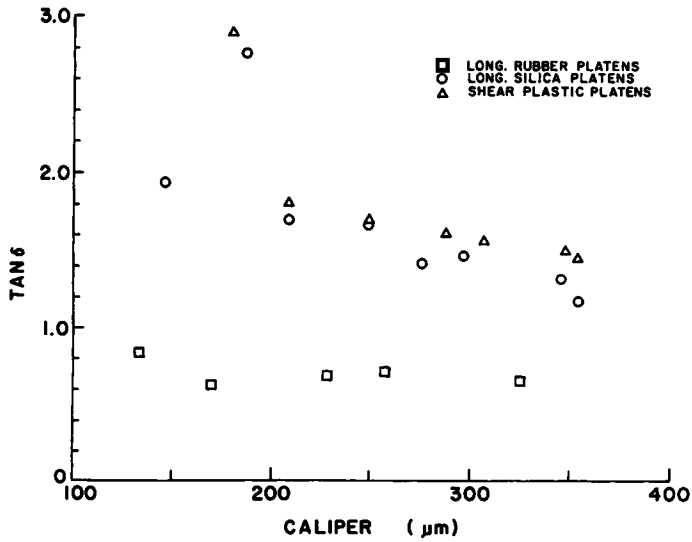

Fig. 3. Loss tangent values, calculated by the McSkimmin method, for the variable basis weight sheets: (□) long rubber platens; (○) long silica platens; (△) shear plastic platens.

Even though the McSkimmin technique did not yield any additional information on sheet properties, the phase velocity measurements do help to evaluate and explain the errors due to insufficient coupling. This is because phase relationships between sinusoidal signals entering and leaving the sample can be analyzed mathematically with transmission line equations. In time-of-flight measurements, distortion at the initial edge of a received pulse makes results difficult to describe mathematically. Since the loss tangent determinations are not feasible, we simplified the McSkimmin technique to a phase determination without an amplitude measurement. We measure the time difference for the arrival of a peak in the sinusoidal wave train far enough into the rf pulse that equilibrium conditions are established. This measurement is made with the hard platen delay line transducers with and without the sample in place. The difference between the two times is divided into the caliper to get an apparent velocity, V_{AP}. The times are taken from the digital readout on the HP oscilloscope, as described in the section on longitudinal time-of-flight measurements. If the paper were homogeneous and its mechanical properties were known, V_{AP} could be calculated (see Appendix A). The result is

$$V_{AP} = \omega/[\text{REAL}(k_s) - \text{PHASE}(E)/l_s] \tag{10}$$

where

$$E = \frac{4Z_T Z_S}{[(Z_T + Z_S)^2 - e^{(-2ik_s l_s)}(Z_T - Z_S)^2]} \tag{11}$$

The function REAL is the real part of the complex number, and PHASE is the phase angle of the complex number. In the results section, eqs. (10) and (11) are modified to take into account a coupling interface between the sample and the delay line. The interface will be given mechanical properties that differ from the bulk of the sample. By comparing experimental values of V_{AP} with theoretical calculations, and assuming different interface properties, explanations for the coupling errors will be evaluated.

RESULTS AND DISCUSSION

When dealing with thin, rough samples, conceptual difficulties confuse the meaning of ZD velocity measurements. Therefore, we begin this section with a discussion of the sheet properties that we are trying to determine when we measure velocity, and a discussion of some of the difficulties that muddle the analysis. First, what do we mean by "thin," and what do we mean by "rough?"

If the wavelength λ of ultrasound in the sample is greater than, or of the order of, the caliper, then the sample is "thin." For our purposes, the thinness (T) is defined as λ divided by the neoprene caliper (l_{SN}). Since wavelength decreases with frequency, it is best to use the highest possible frequency to effectively make the sample thicker. However, if the wavelength decreases to the order of the thickness of a fiber, then much of the ultrasonic energy is lost to scattering by the fibers, and ultrasound does not propagate well

in the sheet. A proper frequency can be chosen to make a sheet "thick" if its caliper is much greater than the lateral dimension of its fibers. For sheets made of typical wood fibers, attenuation due to scattering becomes prohibitive at a few megahertz; therefore, our measurements are made from 0.5 to 1.0 MHz in the shear mode and from 1.0 to 2.0 MHz in the longitudinal mode. These are near the highest frequencies we can use without undue difficulties from scattering.

A sample is rough if the uncertainty in the location of its boundaries is not small compared to its caliper. On a microscopic level, the surface of a sheet is irregular. These irregularities can cause difficulties in coupling acoustic energy into the sheet and distortions in the meaning of the calculated velocity. Since neoprene platens conform to the surface of the sheet much better than hard platens, the difference between standard hard platen caliper (l_{SH}) and neoprene caliper is an indication of surface irregularity. We use this difference divided by the neoprene caliper as a measure of roughness, i.e., "roughness" (R) is defined as $(l_{SH} - l_{SN})/l_{SN}$. If R is small, the complications from poor coupling and from ambiguous caliper definitions can be minimized.

Ultrasound velocity determinations are important because they are nondestructive measures of a mechanical property. More specifically, velocity depends on the elastic and inertial properties of the sample. For the ideal case of a plane wave, of the form $e^{i(\omega t - kx)}$, propagating along a principal direction of an orthotropic medium, the phase velocity ω/k is equal to $(C/\rho)^{1/2}$. Here, C is the elastic stiffness in the principal direction, and ρ is the mass density. Thus, the phase velocity of a plane wave is a measure of specific stiffness, C/ρ. It is this quantity that we are trying to determine when we measure velocity. Any complication due to finite T or R that causes the measured velocity to differ from ω/k must be avoided or taken into account.

If only the difficulties caused by thinness are considered, eqs. (10) and (11) can be used to relate the apparent phase velocity (V_A) to the mechanical properties of the sample. To get this result, it was assumed that the sample was a uniform, smooth-surfaced plate well-coupled to the delay lines; therefore, roughness and poor coupling were ignored. Since we are not attempting to quantitize the loss processes, $\omega/\text{REAL}(k_s)$ is the value we would like to measure. Calling this V, eq. (10) becomes

$$\frac{1}{V} = \frac{1}{V_A} + \frac{\text{PHASE}(E)}{\omega l_s} \tag{12}$$

Thus, $-\text{PHASE}(E)/\omega l_s$ is an inherent error in $1/V_A$, if V_A is taken to be $\omega/\text{REAL}(k_s)$. Since energy is dissipated as sound passes through the sample, k_s is a complex number, and the plane wave, $A_0 e^{i(\omega t - kx)}$, is attenuated as it propagates. The real part of k_s is positive, while the imaginary part is negative. Notice that the second term in the denominator of eq. (11) is a sinusoid that decreases exponentially with l_s. Depending on the value of the quantity in the exponential, this term can result in a positive or negative contribution to phase (E). In fact, as ω progresses, it alternates with a period

in ω of $\pi V/l$, since $\text{REAL}(k_s) = \omega V$. So as ω varies, this term causes $1/V_A$ to oscillate about $1/V$. For a large caliper, this term approaches zero because of the imaginary part of k_s. This oscillation in $1/V_A$ with ω can be thought of as a result of the interference between the component coming straight through the sample and those components reflected between the interfaces before entering the receiver. As ω changes the phase relationship between these components varies, and the combination has alternately more and less phase than the straight-through component. When the caliper is large, the multiple reflections are much more attenuated than the straight-through wave, and the effect is small.

The other term in the denominator of eq. (11) is frequency- and caliper-independent. Looking at E as l_s approaches infinity, we can study the effect of this term:

$$\lim_{l \to \infty} E = \frac{4Z_T Z_S}{(Z_T + Z_S)^2} \tag{13}$$

In our case $Z_T \gg Z_S$, so E simplifies to

$$\lim_{l \to \infty} E \approx \frac{4Z_S}{Z_T} \tag{14}$$

Since Z_T is real, the phase of E can be approximated as

$$\lim_{l_s \to \infty} \text{PHASE}(E) \approx \text{PHASE}(Z_S)$$

and $1/V$ is larger than $1/V_A$ by the amount $\text{PHASE}(Z_S)/\omega l_s$. This term gives a phase shift to the receiver signal that is proportional to the phase of Z_S. As l_s increases, the ratio of this phase shift to the phase shift due to propagation through the sample decreases, and its effect on V_A decreases. This term causes an overestimate of velocity which decreases in magnitude with ωl_s. The phase of Z_S is not zero because of losses in the sample. In fact, $\text{PHASE}(Z_S) = \frac{1}{2}\,\text{PHASE}(C)$, since $Z_S = (\rho C)^{1/2}$. This term originates from noncancellation of phase shifts when a signal is transmitted from delay line to sample and sample to delay line. A straightforward application of transmission line theory shows (see Appendix B) that there is a finite phase shift between a transmitted and an incident wave at the boundary between an elastic and a lossy medium. In addition, the phase shift from elastic to lossy medium does not cancel the shift from lossy to elastic medium, and a net phase shift is produced when a plane wave is transmitted through a lossy plate between elastic delay lines. When $Z_T \gg Z_S$, the net phase shift approaches $-\text{PHASE}(Z_S)$, making V_A greater than V by the same amount as the second term in eq. (11).

For a thin, well-coupled plate, the inherent difference between V and V_A can be attributed to two phenomena: the interference from multiple reflections and a phase shift arising from the lossy nature of the sample. Both effects decrease as frequency and caliper increase. The interference term is reduced by loss in the sample, since multiple reflections are more attenuated

than the straight-through wave. However, the second effect is proportional to the loss angle in the sample. Both of these produce a frequency dependence in the measured value of V_A.

This discussion was directed at phase velocity measurements. The time-of-flight considerations are somewhat different. Since time-of-flight measurements only look at the first half wave striking the receiver, multiple reflections are of concern only if the sample caliper is less than a quarter wavelength, $T > 4.0$. In this case, the first multiple reflection (which must pass through the sample two more times than the primary signal) could interfere in the first half cycle. The lowest frequency used is 0.5 MHz and the highest velocities encountered are about 600 m/s; therefore, there is no need for any worry about multiple reflections in time-of-flight measurement when caliper is greater than 300 μm. The frequency of routine sample characterization is at least 1.0 MHz, and significant interference will occur only when $T > 8$; therefore, a more realistic lower caliper limit is about 100 μm.

The phase shift due to sample losses would be the same in time-of-flight as in phase velocity measurements. This is because the shift in the straight-through component is the same as in a multiple reflection. The ratio of the loss phase shift to the propagation phase shift is $\text{PHASE}(Z_S)/k_s l_s$. From our results with the McSkimmin method, we conclude that the loss tangent in paper is about 0.1. Assuming a maximum ZD velocity of 600 m/s, we find that the error from this term is less than 2% at 1.0 MHz if the caliper is over 200 μm.

From the above considerations, we conclude that time-of-flight measurements on paperboard samples are not significantly affected by multiple reflections or loss phase shifts. However, there are other problems. The shape of the signal in the first half cycle is sensitive to higher order Fourier components in the signal. Further into the pulse, where phase velocity measurements are conducted, the wave can be thought of as a pure sinusoid at the carrier frequency. However, the form of the first half cycle can be distorted by frequency-dependent attenuation and phase velocity in the sample. Relative phase shifts and amplitude shifts between Fourier components as the signal passes through the sample will deform the front edge of the signal. Since attenuation in paper increases with frequency, we expect this dispersion effect to be operative; however, it is difficult to quantify. The dispersion-generated error would be frequency-dependent; most likely, it would increase in magnitude rapidly with frequency.

The experimental results will lead us to conclude that roughness complications are the most important. This is discussed in detail later. However, for the moment we merely state that roughness is like the other difficulties in that it causes a frequency-dependent variation in the measured velocity.

The measurements presented and discussed in this section are taken from 4 types of samples: (1) a 110 lb/1000 ft^2 commercial bleached kraft stock, later referred to as MCS; (2) a 26 lb/1000 ft^2 commercial semichemical corrugating medium with variable surface grinding, called CC76; and (3) a 42 lb/1000 ft^2 commercial unbleached kraft linerboard sample with varying degrees of surface grinding, LB.

The longitudinal results are from time-of-flight measurements using neoprene platens and aluminum foil base times. Three different types of shear

results are reported. Hard platen time-of-flight measurements are called pk. 1 velocities, pillow time-of-flight results are referred to as pillow velocities, and hard platen phase velocities are pk. $\overline{3,4,5}$. The pk. $\overline{3,4,5}$ data are calculated by averaging the apparent velocities for the third, fourth, and fifth peaks. By peak three, the received pulse is close to an equilibrium so that averaging the results for peaks 3, 4, and 5 reduces experimental scatter in the final results. Most of the results presented in this paper are ZD shear. This is because shear coupling is more difficult, making shear the more critical test.

We will look first at the MCS sample. It is about 700 μm in caliper and the depth of its rough surface interface is small compared to its caliper. Figure 4 is a plot of longitudinal ZD velocity for the MCS sample as a function of frequency. As frequency increases, there is a detectable increase in measured velocity. However, the variation is only a few percent, and the results from this sample are relatively frequency-independent. The constancy of the measured velocities with varying frequency is taken as an indication of their validity. This is a sensible criterion, since all conceivable complications result in frequency-dependent errors. Since the MCS values are stable, the ZD longitudinal velocity is taken as a good measure of the specific elastic stiffness of this sample.

Now consider the ZD shear velocity for the MCS sample. Figure 5 shows the three different measures of ZD–CD shear velocity. Notice first the phase velocities (pk. $\overline{3,4,5}$); they seem to oscillate with a small amplitude and constant period around a value of about 350 m/s. This is consistent with the notion of multiple reflections causing oscillations in the measured phase velocities. From eq. (11), the period in frequency of this oscillation should be $V/2l_s$. If this period is taken from the data, V can be roughly calculated. Using an estimate of 0.27 MHz for the period, V is found to be 380 m/s.

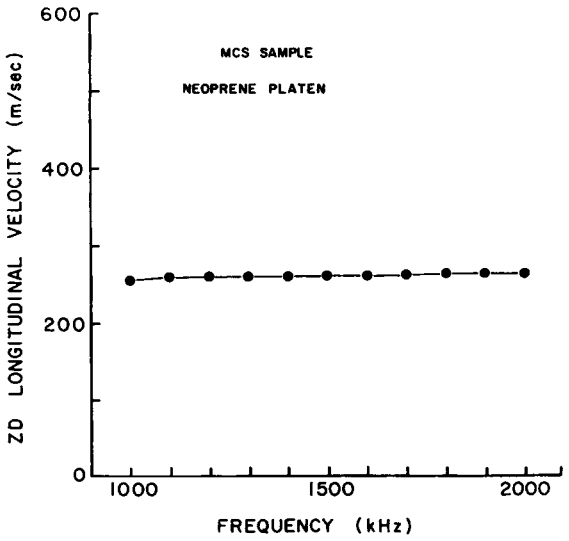

Fig. 4. Neoprene platen, ZD longitudinal velocities vs. frequency for a machine-made bleached kraft paperboard. Hard caliper = 705 μm; neoprene caliper = 692 μm; R = 0.019.

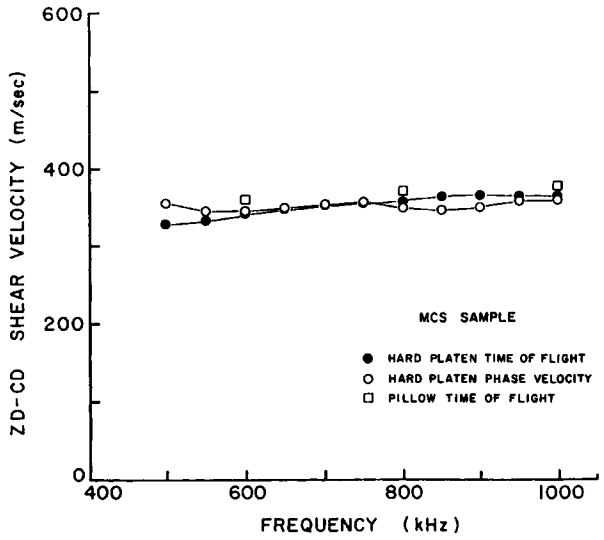

Fig. 5. ZD–MD shear velocity vs. frequency for the MCS sample. Hard platen time of flight (●), pillow time of flight (□), and hard platen pk. $\overline{3,4,5}$ data are shown: (○) hard platen phase velocity.

Within the uncertainty of the period measurement, this is about the same as the 350 m/s average. We conclude that V is near 350 m/s, and that V_A is oscillating about this value due to interferences from multiple reflections. There is not a steady decrease in V_A with frequency, suggesting the phase shifts from sample loss must not be important. The data are behaving as if only multiple reflections are causing V_A to differ from ω/k_s. As expected, the hard platen time-of-flight data (pk. 1) do not show these oscillations. In this case the value of T is much greater than $\frac{1}{4}$ and multiple reflections are not a problem. Since phase shifts from losses do not affect V_A, they should not affect pk. 1 values. However, the velocities do increase with frequency, perhaps reaching a plateau at 365 m/s. This frequency dependence must be due to dispersion or roughness. At any rate, by the time the standard frequency of 1.0 MHz is reached, the pk. 1 values are stable and very near the V_A results. We conclude that the shear velocities at measured 1.0 MHz are good measures of specific stiffness. Notice that the pillow values are always a few percent above the pk. 1 values, presumably because pillow calipers are a few percent less than hard platen calipers. The frequency effect is the same in pillow and hard platen data, indicating that roughness is not the cause. This conclusion is also supported by the lack of obvious roughness effects in V_A.

Now that we have seen what can be expected in a reasonably smooth and thick sample, we will examine the 26 lb/1000 ft^2 corrugating medium. This is the most difficult of all the samples reported. It is relatively thin (about 190 μm), and the roughness factor is around 0.25. Figure 6 is the ZD–MD hard platen shear data vs. frequency for the unground CC76 at four pressures. We observed a rapid increase in signal amplitude with increasing pressure. All data are taken at one typical location on the sample. Notice

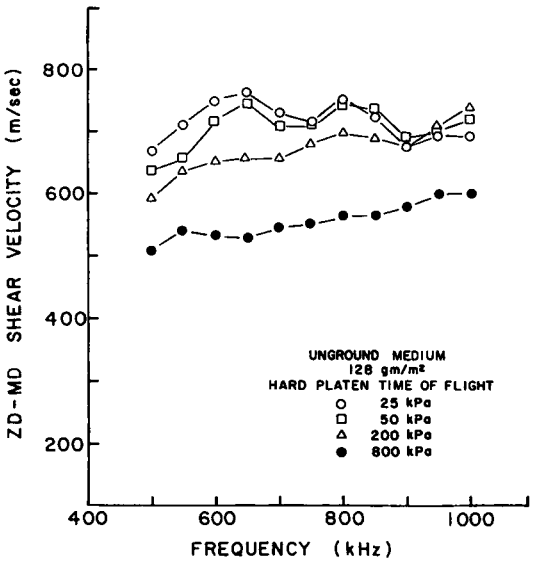

Fig. 6. ZD–MD shear velocity vs. frequency pk. 1 time of flight, hard platen data for unground 26 lb/1000 ft^2 corrugating medium. Data are given for loading pressures of 25 (○), 50 (□), 200 (△), and 800 (●) kPa.

that the variance of velocity with frequency is up to 20%. Oscillations in velocity with frequency also occur, especially at the lower pressures. There is a disconcerting decrease in velocity with pressure. In fact, the actual transit times increase with pressure, even though the caliper is decreasing. The velocities at lower pressure seem unrealistically high.

The pillow data for the same sample are shown in Figure 7. Here the signal amplitude was observed to increase slowly with pressure. The velocity

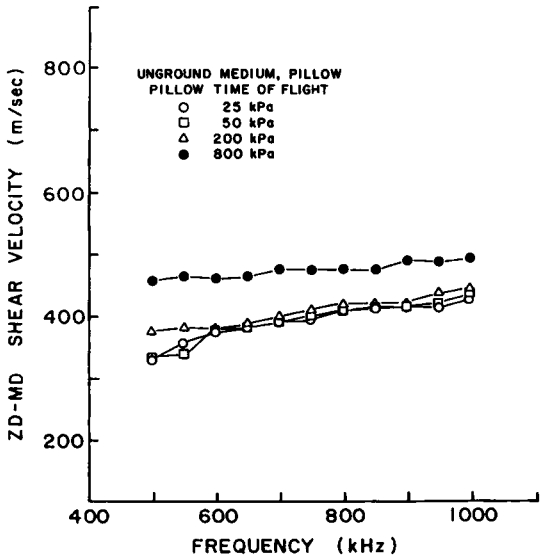

Fig. 7. ZD–MD pillow, pk. 1 data for the unground medium sample of Figure 6.

variations with frequency are reduced, but still significant. Velocity oscillations with frequency are eliminated. The pressure dependence is reversed; velocity increases with pressure, as one would expect. The pk. 1 values are much greater than the pillow values, especially at low pressures. This is the opposite of the MCS sample where the velocity was, understandably, slightly greater with the pillows. The great differences between the pillow and hard platen results decrease with pressure.

Something strange is happening here! The behavior of the hard platen data is irrational in the present context. The pillow data are better, but still not acceptable. The processes already discussed do not account for this behavior. Consider that the samples are thick enough to avoid multiple reflection problems in pk. 1 velocities, that an increase in velocity with frequency is inconsistent with a loss phase shift effect, and that a dispersion explanation could not be expected to account for the differences between pillow and hard platen results. The only remaining option is a roughness effect. To check this possibility, a CC76 sample was surface ground on both sides and the velocity measurements were repeated. The basis weight was reduced from 128 to 114 g/m^2 (only 10%), so that a gross change in sample bulk properties could not be expected. The neoprene caliper was reduced 19%; the hard caliper was reduced 33%; and R went from 28 to 5%. Thus, we had a much smoother sample with approximately the same bulk properties. The hard platen and pillow results are shown in Figures 8 and 9, respectively.

These data are well-behaved compared with the unground sample data. Except for the hard platen data at low pressure, there is little velocity variance with frequency. As with the MCS sample, the pillow velocities are consistently a bit greater than the pk. 1 values. Notice that at high pressures the data for the unground and ground samples are coming into agreement.

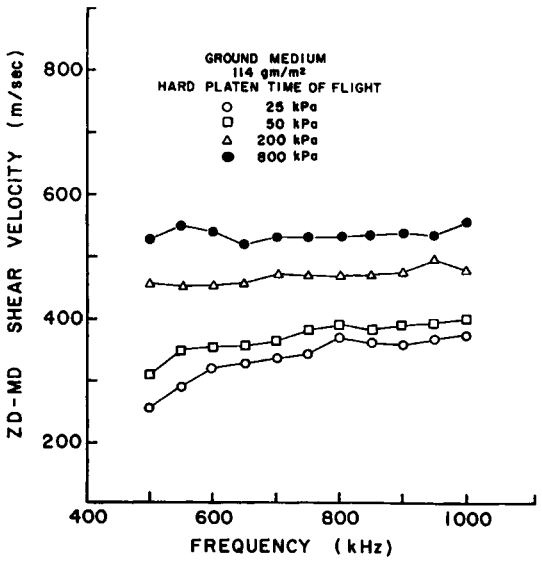

Fig. 8. The same plots as Figure 6 for a medium with a small amount of surface grinding on each side.

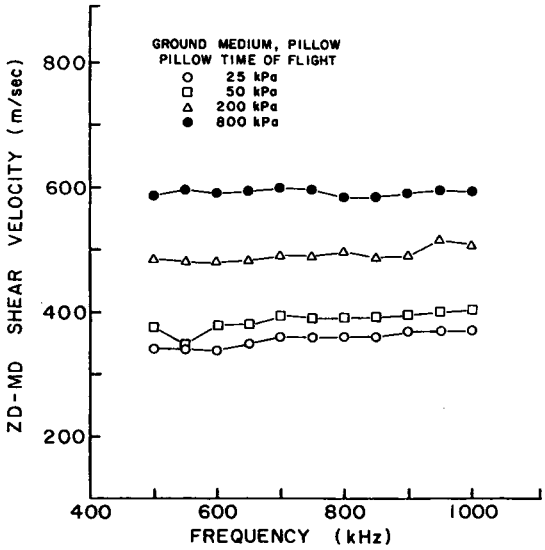

Fig. 9. ZD–MD pillow, pk. 1 data for the ground medium; symbols as in Figure 6.

The pillow data on the ground sheet are stable enough with frequency to assume that they are giving a good measure of specific stiffness. This being the case we observe that specific stiffness increases rapidly with pressure (more about this later). In summary, the difficulty in interpreting the velocity measurements was caused by roughness, since it was removed with a small amount of surface grinding. Coupling with pillows abates the problem, but not completely on this rough medium sample.

Since a small amount of surface grinding on a rough sample greatly changes the magnitude of the velocities and stabilizes their frequency dependence, we conclude that roughness is the major complication. For a sample with a smooth surface our ultrasound velocities are a good measure of specific stiffness if caliper were greater than about 100 μm. Now we are left with two important questions. Why does roughness cause significant changes, and what is so unusual about the surface of paper that in extreme cases transmit times can actually increase with pressure? To understand wave propagation in our thin samples, it is better to deal with plane waves since their action can be described by transmission line equations. Therefore, we will look at the phase velocities of ground and unground medium to see if there is a model of surface roughness consistent with the results. These data are presented in Figures 10 and 11. Notice that the 1.0 MHz values are qualitatively consistent with the corresponding pk. 1 values, but there is much more oscillation in the velocity with frequency, due to the effects of multiple reflections.

The simplest way to account for roughness in phase velocity calculations is to assume that the surface layers have different mechanical properties than the interior. This is done by considering the sample to be made of three transmission lines. The phase difference between the incident wave (E_I) and transmitted wave (E_T) was found in terms of the properties of the delay lines, the sample, and the interfaces, by simplifying the transmission line

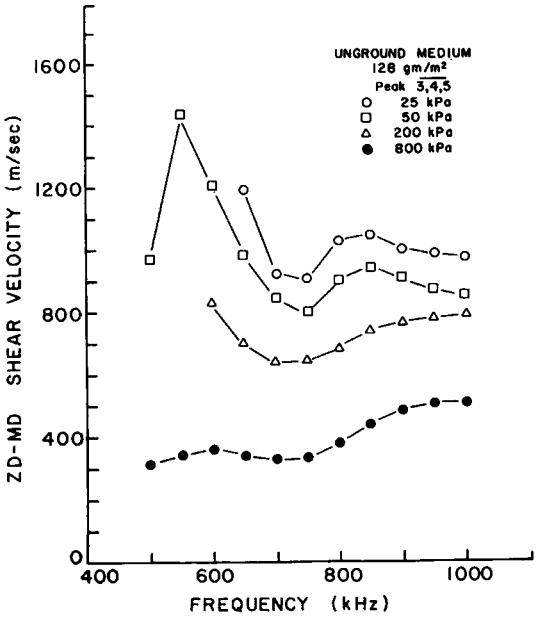

Fig. 10. Hard platen velocity vs. frequency curves for the unground medium calculated by averaging the apparent time of flight for peaks 3, 4, and 5; symbols as in Figure 6.

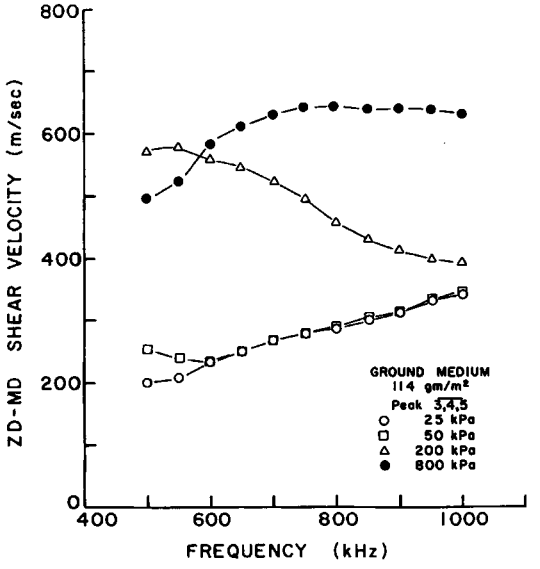

Fig. 11. The same plots as Figure 10 for the ground sample.

equations of Hill and El-Dardiry.[15] The result is that the ratio of E_T to E_I is (see Appendix A)

$$\frac{E_T}{E_I} = 4 \Big/ \left[iS_s\left(\frac{Z_S}{Z_T} + \frac{Z_T}{Z_S} - \frac{Z_I^2}{Z_T Z_S} - \frac{Z_T Z_S}{Z_I^2}\right) + iS_{2I}\left(\frac{2Z_I}{Z_T} + \frac{2Z_T}{Z_I}\right)\right.$$

$$+ iC_{2I}S_s\left(\frac{Z_T}{Z_S} + \frac{Z_S Z_T}{Z_I^2} + \frac{Z_I^2}{Z_S Z_T} + \frac{Z_S}{Z_T}\right) + 4C_{2I}C_s$$

$$- 2S_{2I}S_s\left(\frac{Z_I}{Z_S} + \frac{Z_S}{Z_I}\right)\Bigg] \tag{15}$$

Here l_I is an interface thickness, l_s is the caliper minus $2l_i$, $S_s = \sin(k_s l_s)$, $C_s = \cos(k_s l_s)$, $S_{2I} = \sin(2k_i l_i)$, $C_{2I} = \cos(2k_i l_i)$, Z_S is the interior impedance, and Z_I is the interface impedance. The apparent phase velocity, measured as pk. 3,4,5, is therefore

$$V_A = (l_s + 2l_i)\omega/\text{PHASE}(E_T/E_I) \tag{16}$$

where ω is the angular frequency.

If we make an estimate of the properties of the interface and the interior, we can calculate the phase velocity as a function of frequency. As a first attempt, assume that the surface is bumpy. The intensive properties of the surface and the interior are the same, but the apparent density of the surface is less. So the velocity of ultrasound in the surface and in the interior are equal, and k_s equals k_i. Letting $\rho_i = A\rho_s$, we can plot phase velocity vs. frequency for different values of the coupling coefficient A ($1 \leq A < 0$). These are shown for calipers of 800 and 200 μm in Figures 12 and 13, respectively. The average density is 600 kg/m^3, the velocity throughout is 400 m/s, the loss tangent is zero, and the interface thickness is 40 μm. For the $A = 1.0$ curves, the interface and interior properties are identical, and the resulting

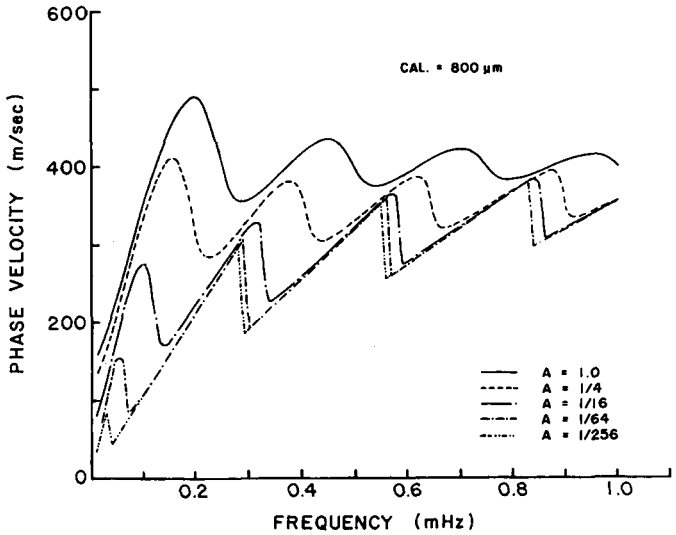

Fig. 12. Theoretical plots of the apparent phase velocity vs. frequency for a 800 μm sample with an apparent density of 600 kg/m^3, an interior phase velocity of 400 m/s, an interface thickness of 40 μm, and a loss tangent of zero. The interface density is A multiplied by 600 kg/m^3, and its phase velocity is also 400 m/s. A: (—) 1.0; (----) 1/4; (–·) 1/16; (–··–) 1/64; (–···–) 1/256.

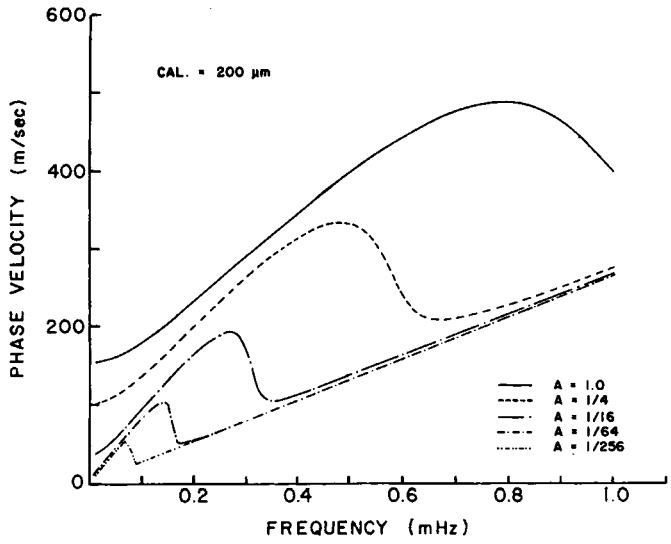

Fig. 13. The same plots as Figure 12 but for a 200 μm thick sample.

curve is that of a smooth sample with no interface. In Figure 14, A is maintained at 0.125, and the thickness of the interfaces varies. Notice first that the interface causes large changes in the theoretical velocity plots, even though the surface and bulk velocities are the same. The effect is generally to lower the velocity and move the oscillations to lower frequencies. Also notice that the experimental curves for the surface ground medium in Figure 11 have the same form as the theoretical curves in Figure 13. Increasing

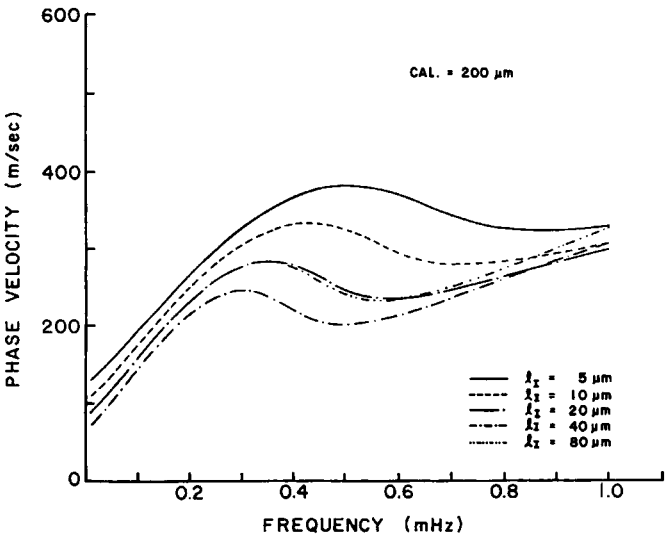

Fig. 14. The effects of interface thickness (l_i) on the theoretical apparent velocity curves. The sample caliper is 200 μm, $V_I = V_S = 400$ m/s, $\rho_s = 600$ kg/m^3, $\tan\delta = 0.4$, $A = 0.125$, and $\rho_i = A\rho_s$. l_I (μm): (—) 5; (----) 10; (-·) 20; (-·-) 40; (···-···) 80.

pressure appears to have the same effect on the experimental curves as increasing A has on the theoretical ones. The theory can be numerically fit to these experimental data quite well by optimizing the interface and interior parameters. However, the fit is not unique due to the large number of independent variables, and this is not a viable method to determine properties. Nonetheless, the theory is helpful in rationalizing the shape of the lower pressure data. It is not so useful in explaining the results on the unground medium. Here, counter to the trend of the theory, the velocity is greatly increased by poor coupling. In fact, there is no apparent way to understand the extremely large measured velocities in terms of this model.

The best way to realize what is happening in the case of the unground medium is to look at it under a microscope. Shives, bundles of unpulped fibers, are scattered throughout the sheet. The extreme extensions of the surfaces are projections of these rigid inhomogeneities. When hard platen transducers are placed on the medium at low pressure, we presume that the transducer to sheet contact occurs only through the shives. The coupling is so poor that little signal is received. The small signal is selectively channeled, however, through the shives, which have a higher velocity than the bulk of the sample. As pressure is increased (or when pillow coupling is used), the amount of bulk material contacting the transducers increases such that the signal amplitude grows, but a smaller portion passes through the shives. In fact, a transit time increase with pressure can be rationalized if the total signal is thought of as an interference between two signals, one part channeled through the shives and the other through the bulk. At low pressure only the part channeled through the shives is present and velocity is large. At higher pressures, this signal is swamped out by the part concentrated in the bulk, and the first signal peak occurs later (even though caliper has decreased) and the velocity can actually decrease.

Some features of the picture can also be incorporated into a three-transmission line model. As before, the interface region will be less dense than the interior, but now the velocity is made greater in the interface. In this way we can model a rough and rigid surface. Figures 15, 16, and 17 use the same bulk properties as the model curves shown in Figures 12, 13, and 14, but the interface regions are given a velocity of 2000 m/s. In Figures 15 and 16, curves for a sheet with no surface layers are included for reference. Notice that the interface region can result in a larger apparent velocity than obtained for the reference if A is not too small. The effect of changing A in Figures 15 and 16 is roughly to project the curves along straight lines through the origin. From Figure 17, we see that large velocities can be achieved by increasing the surface depth. The anomalously large phase velocities found experimentally, and their decrease in severity with improved coupling, are repeated qualitatively in Figure 17. The experimental increase in oscillation frequency with poor coupling, however, is not a feature of theoretical curves. This transmission line model displays some of the characteristics of the phase velocities found for the unground medium samples, but it is not as successful as the rough homogeneous theory was for the ground medium.

Interpretation of the results for the final group of samples is intermediate in difficulty. They are 42 lb/1000 ft^2 linerboards that have had various

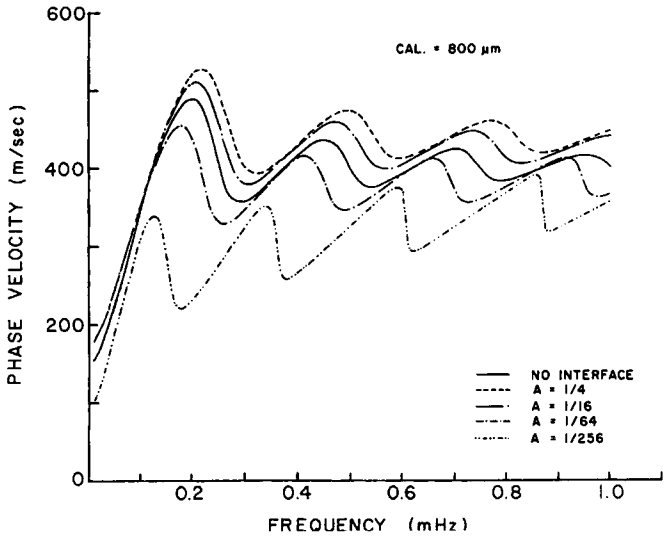

Fig. 15. Theoretical plots of the apparent phase velocity vs. frequency for a 800-μm sample whose interior phase velocity is 400 m/s and surface phase velocity is 2000 m/s. ρ_s = 600 kg/m^2, l_i = 40 μm, tan δ = 0, $\rho_i = A\rho_s$, and $2l_i + l_s$ = 800 μm. (—) No interface; (····) A = 1/4; (–·) A = 1/16; (–·–) A = 1/64; (··–··) A = 1/256.

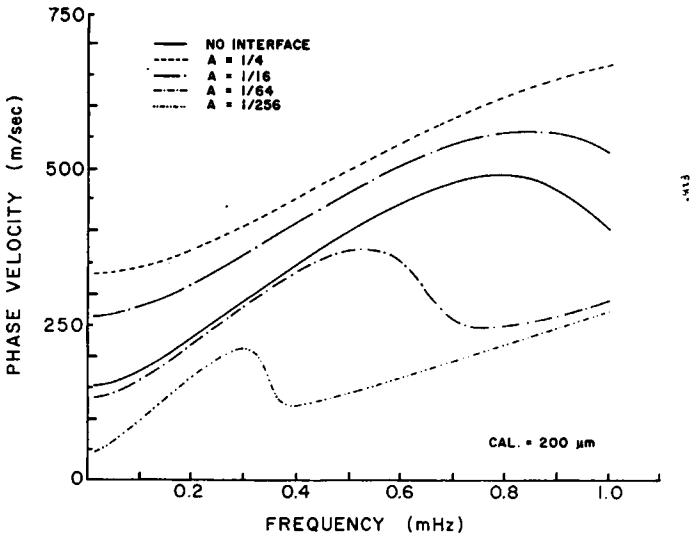

Fig. 16. The same plots as Figure 15 but with caliper of 200 μm.

degrees of surface grinding. This time a significant portion of the sample is taken off (equally on both sides) so that mechanical differences between the exterior and interior of the sample can be studied. The sample marked LB2 is the unground 42 lb/1000 ft^2 stock from which the other samples were produced. Mass and caliper data are given in Table I. The calipers are sheet

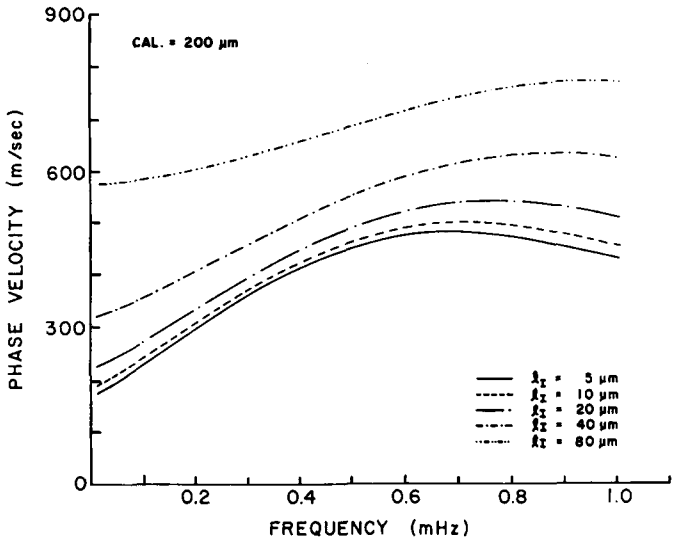

Fig. 17. The same plots as Figure 14 but with the interface velocity V_f equal to 200 m/s.

averages, and they differ slightly from the values on the figures which were taken at single sheet locations. The samples were supplied by Waterhouse,[16] who made similar measurements. His account of the variation in ZD properties is complementary to that given later in this report.

The time-of-flight data for the linerboard series are presented in Figures 18–23, The neoprene ZD longitudinal results are plotted vs. frequency in Figures 18 and 19, for loading pressures of 50 and 200 kPa, respectively. Figures 20, 21, and 22 contain the pk. 1 hard platen shear data on 50, 200, and 800 kPa, respectively. A full velocity vs. frequency curve for pillow data was done only on LB6. This is shown in Figure 23. Pillow data for all samples at 1.0 MHz are in Figure 20. The discrepancy between LB6 velocities at 1.0 MHz in Figures 20 and 23 is a result of using different sample locations.

All the data are reasonably independent of frequency, indicating that a good measure of ω/k is obtained. As pressure increases, coupling improves, and there is less variation with frequency. The pillow data on LB6 are remarkably flat, giving additional confidence in this measurement. At 1.0

TABLE I
Properties of the Linerboard Samples

Sample	Basis weight (g/m^2)	Hard caliper (μm)	Neoprene caliper (μm)	Neoprene density (g/cm^3)	R
LB2	214	325	302	0.71	0.08
LB4	184	272	259	0.71	0.05
LB6	105	208	198	0.69	0.05
LB10	68	107	96	0.71	0.10

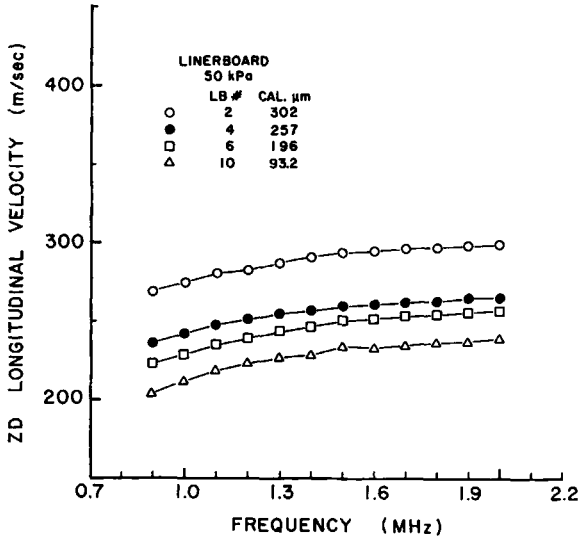

Fig. 18. ZD longitudinal velocity vs. frequency curves for the linerboard series at 50 kPa: (○) LB2; (●) LB4; (□) LB6; (△) LB10.

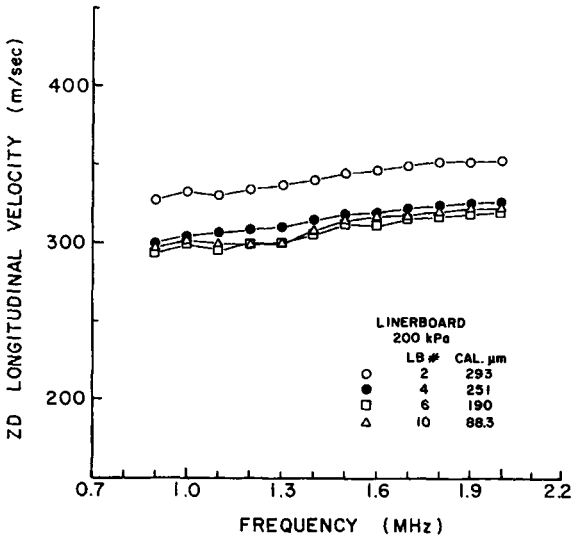

Fig. 19. ZD longitudinal velocity vs. frequency curves for the linerboard series at 200 kPa: (○) LB2; (●) LB4; (□) LB6; (△) LB10.

MHz the hard platen and pillow sheet data agree, except for the unground sheet. Presumably the differences in LB2 velocities arise from the rigid and rough surface effect, similar to, but smaller than that found for the medium sample. The pillow data for LB2 are near that for LB4, and we believe this is a better measure of the average sheet property. There is a larger difference in longitudinal velocity between LB2 and LB4 than found with further surface grinding. This may be due to the presence of a small rigid, rough surface effect, or simply due to uncertainties in sampling.

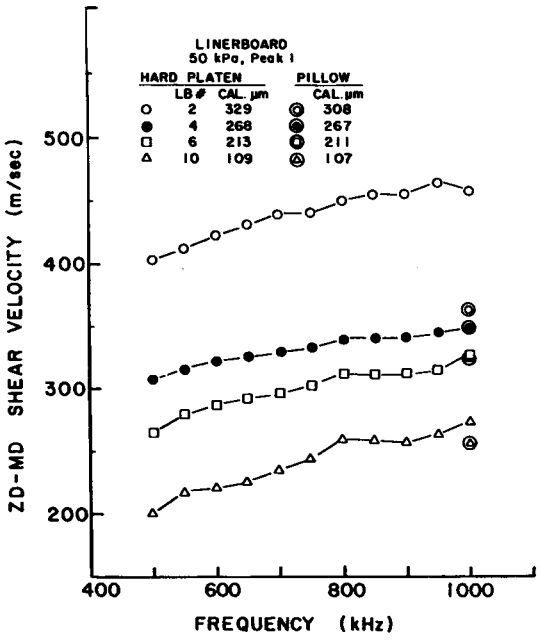

Fig. 20. ZD–MD shear, pk. 1 velocity vs. frequency curves for the linerboard series at 50 kPa: Hard platen: (○) LB2; (●) LB4; (□) LB6; (△) LB10. Pillow (cal μm): (◎) LB2; (⊙) LB4; (▣) LB6; (◬) LB8.

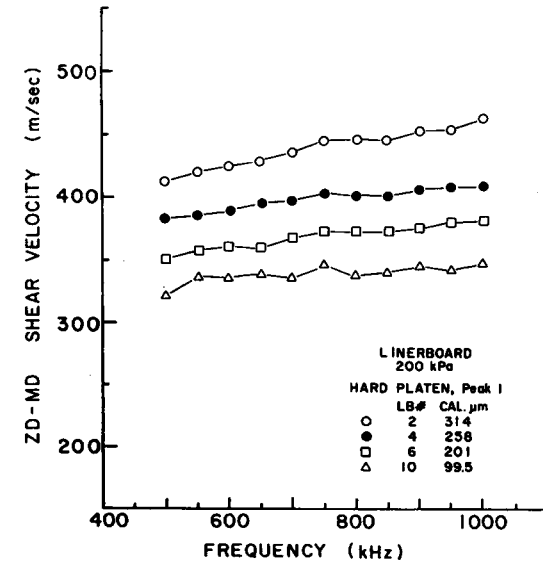

Fig. 21. ZD–MD shear, pk. 1, hard platen velocity vs. frequency curves for the linerboard series at 200 kPa: (○) LB2; (●) LB4; (□) LB6; (△) LB10.

Notice that there is an apparent decrease in velocity toward the center of the sheet. This occurs in both types of measurement but is more pronounced in the shear values. The effect decreases dramatically with pressure. Is this a real phenomenon or is it a result of the technique? The behavior could come from a coupling artifact that is reduced with pressure.

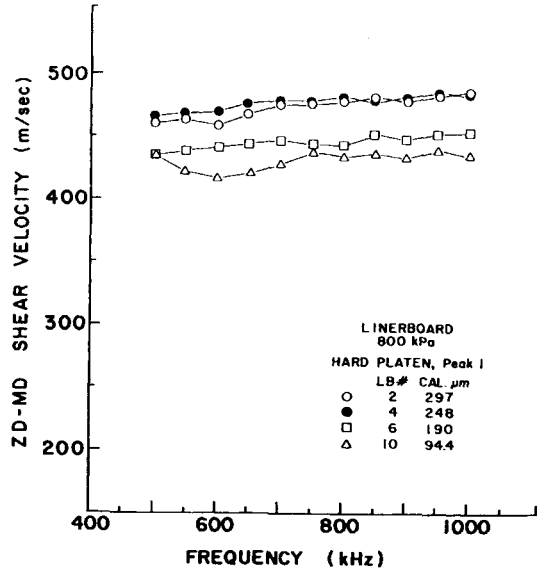

Fig. 22. ZD–MD shear, pk. 1, hard platen velocity vs. frequency curves for the linerboard series at 800 kPa: (○) LB2; (●) LB4; (□) LB6; (△) LB10.

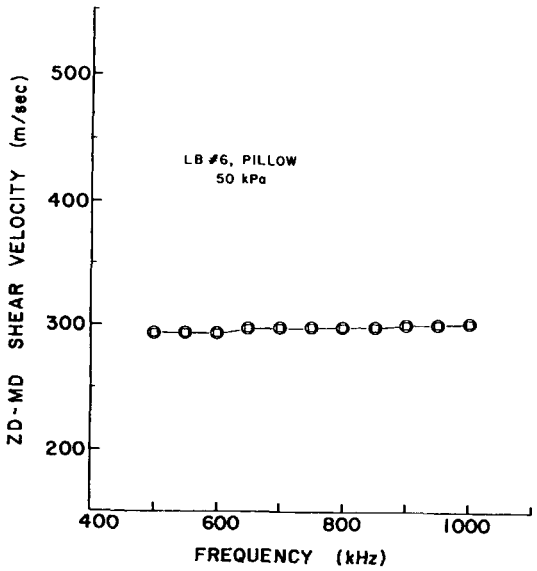

Fig. 23. ZD–MD shear, pk. 1, pillow velocity vs. frequency curves for LB6 at 50 kPa.

However, the relative frequency insensitivity of the data is some evidence of its validity. A similar velocity decrease with grinding occurs in the in-plane velocities, giving us further assurance that the effect is real. There is a 20% increase in the geometric mean of MD and CD in-plane longitudinal velocities when going from LB10 to LB2.[16] Also, the results on the variable

basis weight hand sheets (Fig. 2) showed a decrease in velocity with specimen caliper; however, it was of lower magnitude (about 8% when going from 100 to 300 μm as compared to about 30% for the machine-made linerboard). This is consistent with the observation that no significant in-plane differences were found on the variable basis weight samples. Since there is a corresponding trend with in-plane data, and since velocity can be less sensitive to caliper on less variable samples, we believe that there is a significant decrease in the out-of-plane properties as one goes toward the interior of the sheet.

The velocity in the linerboard samples increases rapidly with pressure, just as it did in the medium. At higher pressures, however, the velocity differences among samples decrease. As pressure rises, the velocities seem to plateau at a common value. This plateau pressure is higher for sections in the center of the sample. It appears that the upper limit of the velocity is the velocity in the fiber cell wall. At low pressures, the loose structure in the sheet results in a low velocity, but as pressure increases the structure tightens and the velocity approaches the velocity of the cell wall. The interior sections are perhaps less bonded and have more open areas, so that higher pressures are required to reach the cell wall velocity. Notice from Table II that there are no significant density differences between the samples.

An interesting exercise is to calculate a ZD wall compressional specific modulus from the caliper change with pressure and to compare this to the ultrasonic values. That is, look at the connections between the change in pressure divided by the change in strain times density and longitudinal velocity squared. These specific moduli are calculated in three ways (using neoprene platens for caliper between 50 and 200 kPa, hard platens between 50 and 200 kPa, and hard platens between 200 and 800 kPa) and listed in Table II, along with the 2.0 MHz average of the longitudinal velocities squared, at 50 and 200 kPa. The values calculated from the caliper changes are much smaller than the ultrasonic velocities, as expected, because of the frequency dependence of elastic moduli in viscoelastic materials. Neoprene results are larger than hard platen results, since neoprene is more conformable and gives a better measure of caliper and changes in caliper. Except for LB2, the trend of lower modulus toward the sheet center is confirmed by this calculation. The lower LB2 values probably arise because of the greater deformation in the rough surface layers in this specimen.

TABLE II
Specific Compressive Moduli from Stress–Strain Measurements

Sample	Average ultrasonic values (m^2/s^2)	Neoprene $\Delta P/(\Delta\varepsilon\rho)$ 50–200 kPa, (m^2/s^2)	Hard $\Delta P/(\Delta\varepsilon\rho)$ 50–200 kPa, (m^2/s^2)	Hard $\Delta P/(\Delta\varepsilon\rho)$ 200–800 kPa, (m^2/s^2)
LB2	1.1×10^5	6.9×10^3	4.4×10^3	1.5×10^4
LB4	8.8×10^4	8.8×10^3	5.4×10^3	2.4×10^4
LB6	8.3×10^4	6.7×10^3	3.6×10^3	1.5×10^4
LB10	8.0×10^4	3.8×10^3	2.8×10^3	1.6×10^4

The apparent phase velocities measured for the LB series are given in Figures 24, 25, and 26. These plots are consistent with the theoretical curves shown in Figures 12–14. With a little imagination, each set of experimental curves can produce one master curve with the shape of a theoretical curve. This is done by shifting the data of the thicker samples to the right and, in

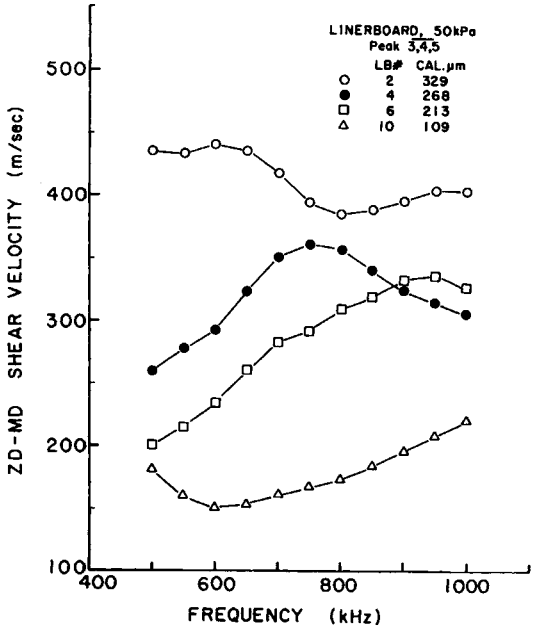

Fig. 24. ZD–MD shear apparent phase velocity vs. frequency curves for the linerboard series at 50 kPa, peak $\overline{3,4,5}$: (○) LB2; (●) LB4; (□) LB6; (△) LB10.

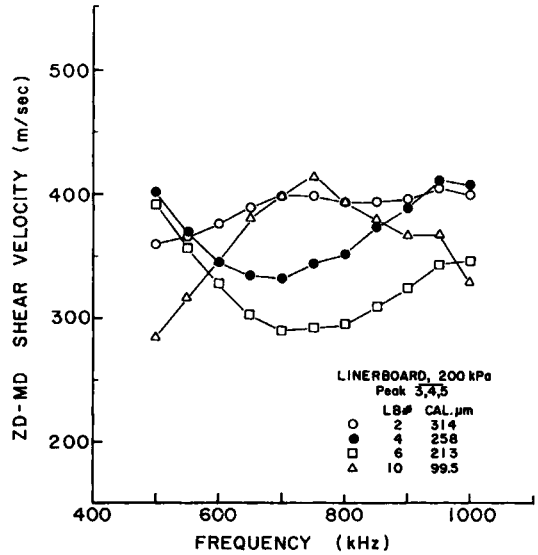

Fig. 25. ZD–MD shear apparent phase velocity vs. frequency curves for the linerboard series at 50 kPa, peak $\overline{3,4,5}$: (○) LB2; (●) LB4; (□) LB6; (△) LB10, 99.5 cal μm.

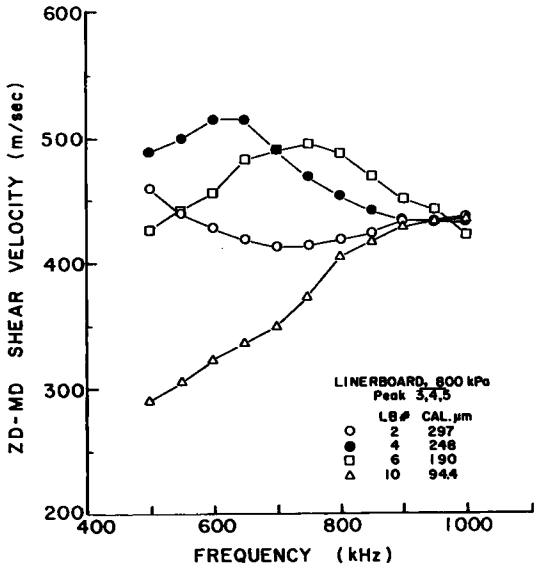

Fig. 26. ZD–MD shear apparent phase velocity vs. frequency curves for the linerboard series at 800 kPa, peak 3,4,5: (○) LB2, 297 cal μm; (●) LB4, 248 cal μm; (□) LB6, 190 cal μm; (△) LB10, 94.4 cal μm.

light of the previous discussion, the data from thinner samples upward. This provides further evidence for the validity of the rough surface model and our conclusions about ZD velocity variations.

CONCLUSIONS

Based on the previous arguments we can now estimate the limits on sample properties that assure valid ZD velocity measurements. Thinness can result in multiple reflection interferences and reduced resolution because of the smaller transit times. For the time-of-flight methods used here, these problems are not serious until caliper is under 100 μm. Therefore, caliper should be at least 100 μm before we can assume that the velocity is a good measure of an average intensive property of the sheet. Roughness, in most cases, is the limiting factor. From our experience, we feel that the R factor (hard caliper minus neoprene caliper divided by neoprene caliper) must be less than 0.1 to avoid serious distortions in the measured velocities due to poor coupling. If R is greater than 0.04, the pillow shear method should be employed. Roughness difficulties can be decreased by increasing the applied pressure. As pressure is increased, however, the results may be more a measure of a cell wall property, and less related to ZD structure.

APPENDIX A: MULTILAYER TRANSMITTANCE CALCULATIONS

Part A. We want to find the ratio of the transmitted pressure (E_t) to the incident pressure (E_i) for a wave of the form $e^{i(\omega t - kx)}$ passing from a material of impedance (Z_t) through a material of length (l_s), wavenumber (k_s) and impedance (Z_s) and back to a material of impedance (Z_t). From Hill and El-Dardiry,[15] eq. (29), this is

$$\frac{E_I}{E_T} = \cos k_s l_s + \frac{i}{2}\left(\frac{Z_S}{Z_T} + \frac{Z_T}{Z_S}\right) \sin k_s l_s \tag{17}$$

For our purposes it is useful to put this in another form. Using Euler's identity ($e^{i\theta} = \cos\theta + i \sin\theta$) to get the sin and cos terms in exponential form, we have

$$\frac{E_I}{E_T} = \frac{1}{2}\left[\frac{e^{ik_s l_s}}{2}\left(2 + \frac{Z_T}{Z_S} + \frac{Z_S}{Z_T}\right) + \frac{e^{-ik_s l_s}}{2}\left(2 - \frac{Z_T}{Z_S} - \frac{Z_S}{Z_T}\right)\right] \tag{18}$$

or

$$\frac{E_T}{E_I} = \frac{4Z_S Z_T}{[e^{ik_s l_s}(Z_T + Z_S)^2 - e^{-ik_s l_s}(Z_T - Z_S)^2]} \tag{19}$$

The transmitted pressure for a traveling wave passing through the S material would change by a factor of $e^{-ik_s l_s}$. Therefore, the phase of $E_T/(E_I e^{-ik_s l_s})$ is the additional phase shift due to nonpropagation phase changes. Calling this term E, we have

$$E \equiv \frac{E_T e^{ik_s l_s}}{E_I} = \frac{4Z_S Z_T}{[(Z_T + Z_S)^2 - e^{-2ik_s l_s}(Z_T + Z_S)^2]} \tag{20}$$

The actual phase shift in going across S is PHASE(E) − REAL($k_s l_s$). Therefore, the time difference between points of equal phase is found from

$$wt - \text{REAL}(k_s l_s) + \text{PHASE}(E) = 0 \tag{21}$$

or

$$t = [\text{REAL}(k_s l_s) - \text{PHASE}(E)]/\omega \tag{22}$$

The apparent velocity (V_A) would be l_s/t, so that

$$V_A = \frac{\omega}{\text{REAL}(k_s) - \text{PHASE}(E)/l_s} \tag{23}$$

If the true velocity (V) is defined as $\omega/\text{REAL}(k_s)$, then

$$\frac{1}{V_A} = \frac{1}{V} - \frac{\text{PHASE}(E)}{\omega l_s} \tag{24}$$

Part B. Now we expand the three layer case of Part A to five layers by adding two interface layers with impedance (Z_I), length (l_i), and wavenumber k_i. One interface layer is inserted between each T to S coupling. Now we need to know both E_R/E_T and E_I/E_T. From Hill and El-Dardiry,[15] eq. (33), we have

$$\begin{pmatrix} E_I + E_R \\ \dfrac{E_I - E_R}{Z_T} \end{pmatrix} = \begin{pmatrix} C_I & iZ_I C_I \\ \dfrac{iS_I}{Z_I} & C_I \end{pmatrix}\begin{pmatrix} C_S & iZ_S Z_S \\ \dfrac{iS_S}{Z_S} & C_S \end{pmatrix}\begin{pmatrix} C_I & iZ_I C_I \\ \dfrac{iS_I}{Z_S} & C_I \end{pmatrix}\begin{pmatrix} E_T \\ \dfrac{E_T}{Z_T} \end{pmatrix} \tag{25}$$

where $C_I = \cos k_i l_i$, $S_I = \sin k_i l_i$, $C_S = \cos k_s l_s$, and $S_S = \sin k_s l_s$. Doing the matrix multiplication gives

$$\begin{pmatrix} E_I + E_R \\ \dfrac{E_I - E_R}{Z_T} \end{pmatrix} = \begin{pmatrix} (C_I^2 - C_S^2)C_S - \left(\dfrac{Z_I}{Z_S} + \dfrac{Z_S}{Z_I}\right) S_I C_I S_S & 2iZ_I S_I C_S + iZ_S C_I^2 S_S - \dfrac{iZ_I^2}{Z_S} S_I^2 S_S \\ \dfrac{2iC_I C_S S_I}{Z_I} + \dfrac{iC_I^2 S_S}{Z_S} - \dfrac{iZ_S S_I^2 S_S}{Z_I^2} & (C_I^2 - C_S^2)C_S - \left(\dfrac{Z_I}{Z_S} + \dfrac{Z_S}{Z_I}\right) S_I C_I S_S \end{pmatrix} \begin{pmatrix} E_T \\ \\ Z_T \end{pmatrix} \tag{26}$$

Solving this for E_R/E_I produces

$$\frac{E_R}{E_T} = \frac{i}{2}\left[S_S C_I^2 \left(\frac{Z_S}{Z_T} - \frac{Z_T}{Z_S}\right) + S_S S_I^2 \left(\frac{Z_S Z_T}{Z_I^2} - \frac{Z_I^2}{Z_S Z_T}\right) + 2C_S C_I S_I \left(\frac{Z_I}{Z_T} - \frac{Z_T}{Z_I}\right)\right] \tag{27}$$

Solving for E_I/E_T yields

$$\frac{E_I}{E_T} = C_S(C_I^2 - S_I^2) - \left(\frac{Z_I}{Z_S} + \frac{Z_S}{Z_I}\right) S_S S_I C_I + i\left[C_S C_I S_I \left(\frac{Z_I}{Z_T} + \frac{Z_T}{Z_I}\right) + \frac{1}{2} S_S C_I^2 \left(\frac{Z_S}{Z_T} + \frac{Z_T}{Z_S}\right) - \frac{1}{2} S_I^2 S_S \left(\frac{Z_I^2}{Z_S Z_T} + \frac{Z_S Z_T}{Z_I^2}\right)\right] \tag{28}$$

APPENDIX B: THE PHASE SHIFT FROM SAMPLE LOSSES

We want to find the net phase shift due to transmission from a high impedance, elastic medium (the delay line) to a low impedance, lossy medium (the sample) and their transmission into the other delay line. The ratio of a transmitted pressure wave (E_T) to the incident wave (E_I), at the delay line to sample interface, is

$$\left(\frac{E_T}{E_I}\right)_1 = \frac{2Z_S}{Z_S + Z_T} \tag{29}$$

Here, Z_S is the complex impedance of the lossy sample and Z_T (a real number) is the impedance of the delay line. The ratio for transmissions from the sample to delay line is

$$\left(\frac{E_T}{E_I}\right)_2 = \frac{2Z_T}{Z_S + Z_T} \tag{30}$$

Writing Z_S in terms of its real and imaginary parts, Z_S' and Z_S'', the phase shifts at the two interfaces are

$$\phi_1 = \text{PHASE}\left(\frac{2Z_S' + 2iZ_S''}{Z_T + Z_S' + iZ_S''}\right) \tag{31}$$

and

$$\phi_2 = \text{PHASE}\left(\frac{2Z_T}{Z_T + Z_S' + iZ_S''}\right) \tag{32}$$

Multiplying numerators and denominators by the complex conjugates of the denominators simplifies eqs. (31) and (32) to the following equations:

$$\phi_1 = \tan^{-1}\left[\frac{Z_T Z''_S}{Z'_S(Z_T + Z'_S) + Z''_S Z''_S}\right] \tag{33}$$

$$\phi_2 = \tan^{-1}\left(\frac{-Z''_S}{Z_T + Z'_S}\right) \tag{34}$$

Assuming $Z_T \gg |Z_S|$, eqs. (33) and (34) become

$$\phi_1 \approx Z''_S/Z'_S = \text{PHASE}(Z_S) \tag{35}$$

$$\phi_2 \approx 0 \tag{36}$$

The two phase shifts do not cancel, and a net phase shift equal to 0.5 tan δ arises from the transmission across the interfaces.

References

1. J. K. Craver and D. L. Taylor, *Tappi*, **48**(3), 142 (1965).
2. J. K. Craver and D. L. Taylor, *Pulp Paper Mag. Can.*, **67**(7), T332 (1967).
3. M. Jackson and G. Gavelin, *Svensk Papperstid.*, **70**(3), 63 (1967).
4. G. A. Baum and L. R. Bornhoeft, *Tappi*, **62**(5), 87 (1979).
5. C. C. Habeger, R. W. Mann, and G. A. Baum, *Ultrasonics*, **17**(2) 57 (1979).
6. R. W. Mann, G. A. Baum, and C. C. Habeger, *Tappi*, **62**(8), 115 (1979).
7. R. W. Mann, G. A. Baum, and C. C. Habeger, *Tappi*, **63**(2), 163 (1980).
8. G. A. Baum, D. G. Brennan, and C. C. Habeger, *Tappi*, **64**(9), 97 (1981).
9. E. H. Fleischman, G. A. Baum, and C. C. Habeger, *Tappi*, **65**(10), 115 (1982).
10. C. C. Habeger and W. J. Whitsitt, *Fiber Sci. Technol.*, **19**(3), 151 (1983).
11. M. Luukkala, P. Heikkila, and J. Surakka, *Ultrasonics*, **9**, 201 (1971).
12. K. W. Hardacker, Internal Report at The Institute of Paper Chemistry (available upon request).
13. W. A. Wink and G. A. Baum, *Tappi*, **66**(9), 131 (1983).
14. H. J. McSkimmin, *J. Acoust. Soc. Am.*, **23**(4), 429 (1951).
15. R. Hill and S. M. A. El-Dardiry, *J. Acoust. Soc. Am.*, **67**(2), 673 (1980).
16. J. Waterhouse, "Out-of-Plane Shear Deformation Behavior of Paper and Board," Project 3500, Progress Report One, The Institute of Paper Chemistry, 1983.

Received October 31, 1985
Accepted November 13, 1985